

**Vortex Induced Vibration (VIV) Based Electro-mechanical Energy
Harvesting System in Confined Space**



Author

HANZLA SHAHID

Regn Number

NUST2021-MSME-00000363722

Supervisor

Dr. EMAD UDDIN

DEPARTMENT OF MECHANICAL ENGINEERING
SCHOOL OF MECHANICAL & MANUFACTURING ENGINEERING
NATIONAL UNIVERSITY OF SCIENCES AND TECHNOLOGY
ISLAMABAD, PAKISTAN

JUNE 23, 2023

**Vortex Induced Vibration (VIV) Based Electro-mechanical Energy
Harvesting System in Confined Space**

Author

HANZLA SHAHID

Regn Number

NUST2021-MSME-00000363722

A thesis submitted in partial fulfillment of the requirements for the degree of
MS Mechanical Engineering

Thesis Supervisor:

Dr. Emad Uddin

Thesis Supervisor's Signature: _____

**DEPARTMENT OF MECHANICAL ENGINEERING
SCHOOL OF MECHANICAL & MANUFACTURING ENGINEERING
NATIONAL UNIVERSITY OF SCIENCES AND TECHNOLOGY,
ISLAMABAD, PAKISTAN**

JUNE 23, 2023

MASTER THESIS WORK

We hereby recommend that the dissertation prepared under our supervision by: Hanzla Shahid (2021-MSME-363722)

Titled: Vortex Induced Vibration (VIV) Based Electro-mechanical Energy Harvesting System in Confined Space

be accepted in partial fulfillment of the requirements for the award of degree.

Examination Committee Members


1. Name: Dr. Zaib Ali

Signature: 

2. Name: Dr. Adnan Munir

Signature: 

3. Name: Dr. Izhar Ullah

Signature: 

Supervisor's name: Dr. Emad Uddin

Signature: 

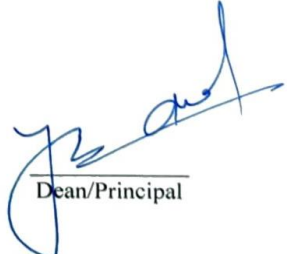
Date: 3-7-23


Head of Department

3-7-23
Date

COUNTERSIGNED

Date: 3-7-23


Dean/Principal


Thesis Acceptance Certificate

Certified that final copy of MS thesis written by Hamza Shahid Registration No. 2021-MSME-363722, of SMME has been vetted by undersigned, found complete in all respects as per NUST Statutes / Regulations, is free of plagiarism, errors, and mistakes and is accepted as partial fulfillment for award of MS degree. It is further certified that necessary amendments as pointed out by GEC members of the scholar have also been incorporated in the said thesis.

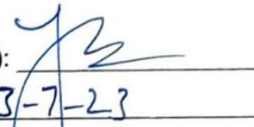
Signature: 

Name of Supervisor: Dr. Emad Uddin

Date: 23/06/2023

Signature (HOD): 

Date: 3-7-23

Signature (Principal): 

Date: 3-7-23

Certificate for Plagiarism

It is certified that MS Thesis Titled: **Vortex Induced Vibration (VIV) Based Electro-mechanical Energy Harvesting System in Confined Space** by **Hanzla Shahid (NUST2021-MSME-00000363722)** has been examined by me. I undertake the follows:

- a. Thesis has significant new work/knowledge as compared to already published or are under consideration to be published elsewhere. No sentence, equation, diagram, table, paragraph, or section has been copied verbatim from previous work unless it is placed under quotation marks and duly referenced.
- b. The work presented is original and own work of the author (i.e., there is no plagiarism). No ideas, processes, results, or words of others have been presented as Author own work.
- c. There is no fabrication of data or results which have been compiled/analyzed.
- d. There is no falsification by manipulating research materials, equipment, or processes, or changing or omitting data or results such that the research is not accurately represented in the research record.
- e. The thesis has been checked using TURNITIN (copy of originality report attached) and found within limits as per HEC plagiarism Policy and instructions issued from time to time.

Name & Signature of Supervisor

Dr. Emad Uddin

Signature: _____

Declaration

I certify that this research work titled “*Vortex Induced Vibration (VIV) Based Electro-mechanical Energy Harvesting System in Confined Space*” is my own work. The work has not been presented elsewhere for assessment. The material that has been used from other sources has been properly acknowledged / referred.

Hanzla Shahid

NUST2021-MSME-00000363722

Copyright Statement

- Copyright in text of this thesis rests with the student author. Copies (by any process) either in full, or of extracts, may be made only in accordance with instructions given by the author and lodged in the Library of NUST School of Mechanical & Manufacturing Engineering (SMME). Details may be obtained by the Librarian. This page must form part of any such copies made. Further copies (by any process) may not be made without the permission (in writing) of the author.
- The ownership of any intellectual property rights which may be described in this thesis is vested in NUST School of Mechanical & Manufacturing Engineering, subject to any prior agreement to the contrary, and may not be made available for use by third parties without the written permission of the SMME, which will prescribe the terms and conditions of any such agreement.
- Further information on the conditions under which disclosures and exploitation may take place is available from the Library of NUST School of Mechanical & Manufacturing Engineering, Islamabad.

Acknowledgements

I would like to begin by expressing my heartfelt gratitude to **Allah Subhan Tallah**, my Creator, for His continuous guidance and blessings throughout the duration of this work. Without His unwavering support and the inspiration, He has bestowed upon me, I would not have been able to enhance my research. All praise and thanks are solely due to Allah Subhan Tallah.

I feel great pleasure in extending my heartfelt gratitude to my supervisor, **Dr. Emad Uddin**, for his tireless efforts and continuous motivation. I would also like to thank **Dr. Usman Latif, Dr. Zaib Ali, Dr. Adnan Munir** and **Dr. Izhar Ullah** for being on my thesis guidance and evaluation committee.

I would like to express my sincere appreciation to my parents, **Shahid Aziz** and **Shabana Naheed**, for their constant love, support, and unwavering belief in my abilities. They have been my pillars of strength, providing guidance and encouragement at every step of my academic pursuits.

Furthermore, I extend my heartfelt gratitude to my beloved brothers **Haris Shahid** and **Muhammad Umar Shahid** for their unwavering support and encouragement. Their belief in my abilities and constant presence have been a source of motivation throughout this endeavor.

My special thanks are due for my dearest maternal Uncle **M. Ismail Ghazi**, close friends **Hafiz Hamza Riaz, Adeel Javed** and **Muhaiman Waheed** for their insistence in my pursuit of higher education when I was confused to take the decision for higher studies. Their timely advice, constant support and belief in my potential have played a significant role in shaping my aspirations.

I am also immensely grateful to **Mahad Shah**, a Ph.D. student in the flow visualization lab, for his invaluable assistance and unwavering support in resolving problems related to lab experimentation. His expertise and availability whenever I faced challenges have been indispensable to the successful completion of my thesis. I deeply appreciate his dedication and assistance throughout this research journey.

I am also grateful to the members of my thesis guidance and evaluation committee for their valuable input and feedback, which greatly contributed to the improvement of my research.

Finally, I extend my thanks to all the individuals who have helped throughout my study. Their contributions, whether big or small, have played a significant role in the successful completion of my thesis.

Dedicated to my exceptional parents, maternal uncle and adored brothers whose tremendous support and cooperation led me to this wonderful accomplishment.

Abstract

The increasing global demand for sustainable and efficient energy sources due to environmental concerns is pressing. Energy harvesting from fluid flows provides a promising option for renewable energy generation, and the development of self-sustaining devices is crucial for practical implementation. In this regard, the need to study the impact of varying the size of bound region on energy harvesting is necessary, which is significant for the optimal design of portable devices due to the establishment of boundary layer. Therefore, this experimental study aims to investigate the effect of changing the distance between wall boundaries on the performance of a piezoelectric-based energy harvester in generating electrical energy from fluid flow. A series of experiments were conducted to analyze the dynamical behavior of a piezoelectric flag due to gap variation and the impact of boundary layer thickness (δ) on its behavior. The setup involved placing inverted C-shaped (120-degree cut) and circular cylinders in a uniform fluid flow, utilizing the undulating motion of the piezo flag in the downstream vortices to harvest electrical energy. The distinct flapping modes were observed in the experimental results which can create varying degrees of coupling in the wake flow. The dynamic behavior of the piezoelectric flag was observed to be influenced by both the gap between cylinder and flag (D_x) and Cylinder to wall (D_y), leading to output power fluctuation. For each x^* value, the power output levels were analyzed by experimentally varying D_x values from 1.0 to 5.0 for different values of D_y in terms of δ to find the optimal configuration. The cylindrical arrangement of both bluff bodies, characterized by $D_y = 34.05\delta$ and $x^* = 310$ mm, exhibits a persistent pattern of peak power output within the range of $2.0 \leq D_x \leq 3.0$ due to continuous flapping and significant amplitudes. The inverted C-shaped cylinder (120° cut) shows a maximum gain of 83% in power output compared to the circular cylinder. Furthermore, it is demonstrated that certain spanwise gaps lead to low energy production due to boundary viscous effects and poor coupling of wake flow. This study provides valuable insights into the development of more efficient and optimal sustainable devices for remote practical applications and renewable energy sources, reducing dependence on conventional sources.

Key Words: *Energy harvesting, Piezoelectric-flag, Vortex Induced Vibration (VIV), Particle Image Velocimetry (PIV), Boundary layer thickness*

Table of contents

CHAPTER 1	14
INTRODUCTION	14
1.1 Piezoelectricity: An overview	15
1.1.1 Quartz	16
1.1.2 Ceramics	16
1.1.3 Polymers	16
1.1.4 Composite materials	17
1.2 Reasons for choosing PVDF Flag	17
1.3 Motivation	17
1.4 Research Aim	18
1.5 Research Objectives/Limitations.....	18
1.5.1 Objectives	18
1.5.2 Limitations.....	19
1.6 Structure of thesis.....	19
CHAPTER 2	20
2.1 Introduction	20
2.2 Energy harvesting using FIV technique	21
2.3 Energy harvesting in Tandem configuration	22
2.4 Geometrical shapes	23
2.5 Novelty of this research.....	24
CHAPTER 3	26
3.1 Water Tunnel Setup.....	26
3.2 Particle image Velocimetry	31
CHAPTER 4	35
4.1 Performance and Response of harvester for different geometrical cross sections.....	37
4.1.1 Experimental Measurements using circular cylinder as bluff body at distance of 360 mm between plates	37
4.1.2 Experimental Measurements using 120 degree cut C-type cylinder as bluff body at distance of 360 mm between plates.....	38

4.1.3	Experimental Measurements using circular cylinder as bluff body at distance of 310 mm between plates	40
4.1.4	Experimental Measurements using circular cylinder as bluff body at distance of 310 mm between plates	41
4.1.5	Experimental Measurements using circular cylinder as bluff body at distance of 260 mm between plates	43
4.1.6	Experimental Measurements using 120° cut inverted C-type cylinder as bluff body at distance of 260 mm between plates.....	44
4.2	Comparative Analysis and Optimal Configuration	45
Chapter 5	50
Conclusion	50
References	51

List of Figures

Fig 1: Categorization of sources of renewable energy.....	14
Fig. 2: (a) Inverse and direct piezo effect (b) Cell structure of piezo film.....	16
Fig. 3: Real Time experimental setup of water channel.....	27
Fig. 4: Schematic of complete experimental setup.....	28
Fig. 5: A schematic of the experimental setup is depicted, showing a flag that is clamped at its leading end and free at its trailing end (top view) (a) Circular cylinder (b) 120 degree cut C-type inverted cylinder.	30
Fig. 6: Details of cantilevered flag.....	31
Fig. 7: Schematic for PIV System.....	32
Fig. 8: Real time setup for PIV.....	33
Fig. 9: (a) Variation of Non-dimensional peak amplitude and flapping envelope for high energy output configuration at $D_x = 3$ and $D_y = 34.05\delta$ (b) Variation of Non-dimensional peak amplitude and flapping envelope for high energy output configuration at $D_x = 5$ and $D_y = 18.96 \delta$	36
Fig. 10: (a) Power output (b) non-dimensional flapping amplitude (c) dominant frequency for circular cylinder for streamwise gaps ($D_x = 1-5$) and spanwise gaps ($13.22 \leq D_y / \delta \leq 52.89$) for $x^* = 360$ mm at constant velocity.....	38
Fig. 11: (a) Power out (b) non-dimensional flapping amplitude (c) dominant frequency for 120° cut inverted C-type cylinder for streamwise gaps ($D_x = 1-5$) and spanwise gaps ($13.22 \leq D_y / \delta \leq 52.89$) for $x^* = 360$ mm at constant velocity.....	39
Fig. 12: (a) Power out (b) non-dimensional flapping amplitude (c) dominant frequency for circular cylinder for streamwise gaps ($D_x = 1-5$) and spanwise gaps ($11.35 \leq D_y / \delta \leq 45.41$) for $x^* = 310$ mm at constant velocity.	41
Fig. 13: (a) Power out (b) non-dimensional flapping amplitude (c) dominant frequency for 120° cut inverted C-type cylinder for streamwise gaps ($D_x = 1-5$) and spanwise gaps ($11.35 \leq D_y / \delta \leq 45.41$) for $x^* = 310$ mm at constant velocity.....	42
Fig. 14: (a) Power out (b) non-dimensional flapping amplitude (c) dominant frequency for circular cylinder for streamwise gaps ($D_x = 1-5$) and spanwise gaps ($9.48 \leq D_y / \delta \leq 37.92$) for $x^* = 260$ mm at constant velocity.	44

Fig. 15: (a) Power out (b) non-dimensional flapping amplitude (c) dominant frequency for 120° cut inverted C-type cylinder for streamwise gaps ($D_x = 1-5$) and spanwise gaps ($9.48 \leq D_y / \delta \leq 37.92$) for $x^* = 260$ mm at constant velocity..... 45

Fig. 16: (a) Power, A/L ratio and Flapping Frequency for maximum configuration among all for circular cylinder at point $D_x = 3, D_y = 34.05\delta$ for $x^* = 310$ mm (b) Power, A/L ratio and Flapping Frequency for maximum configuration among all for 120° degree cut C-type..... 47

Fig. 17: (a) RMS and Instantaneous Voltage for maximum output configuration for 120° cut C-type inverted cylinder at point $D_x = 3, D_y = 34.05\delta$ for $x^* = 310$ mm (b) RMS and Instantaneous Voltage for minimum output configuration for circular cylinder at point $D_x = 5, D_y = 18.96\delta$ for $x^* = 260$ mm..... 47

Fig. 18: PIV Result for maximum and minimum energy generation cases taken by taking the average of 1000 images 49

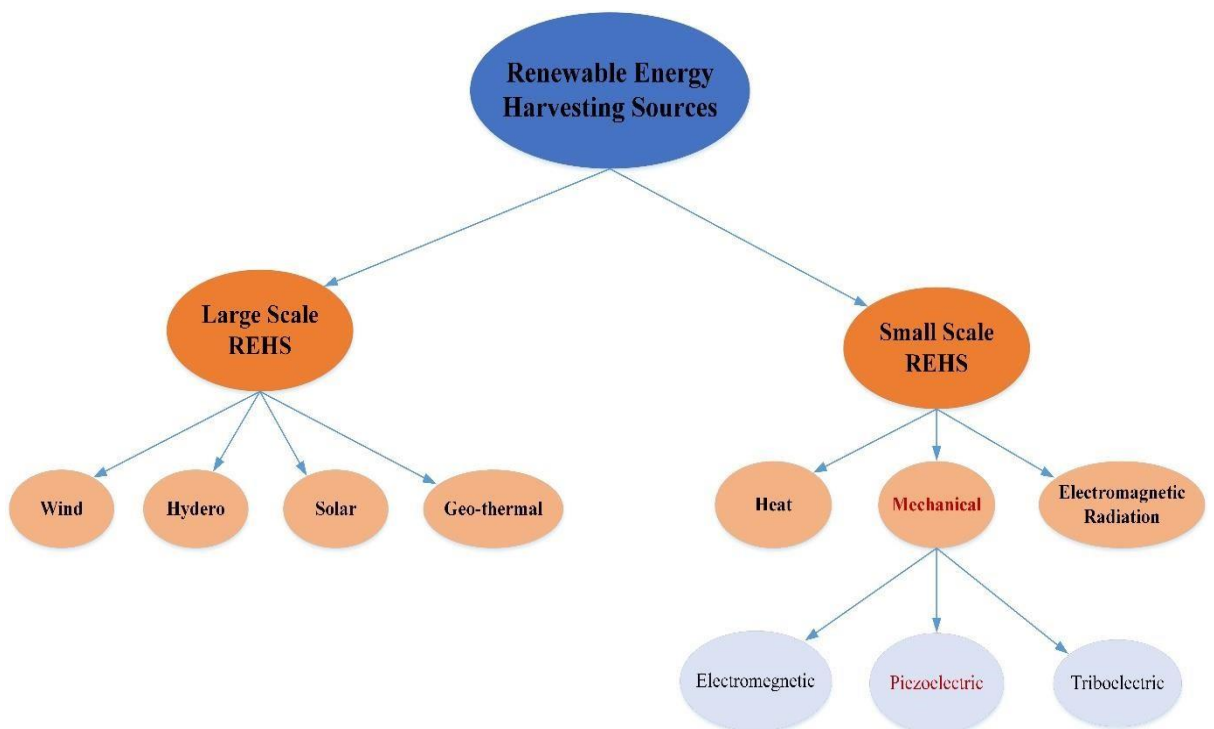
List of Tables

Table 1	29
Table 2	29

CHAPTER 1

INTRODUCTION

Energy harvesting is a cutting-edge method created to supply electrical energy to remote sources, particularly for running low-powered wireless sensors and electronic equipment. In addition to facilitating wireless health monitoring applications, these energy harvesting systems can help with the production of renewable energy. By replacing traditional battery packs and decreasing chemical and hazardous waste, they also improve the environment. The development of energy harvesting has been considerably aided by the ongoing advancements in research on Internet of Things (IoT) devices, wearable electronics, smart infrastructure, environmental monitoring, and healthcare applications [1–3]. The weight and volume of the batteries used in these systems have a significant impact on both their design lifespan and performance [4]. The key energy sources suitable for energy harvesting devices in various application sectors, according to notable studies [5–7] are ambient flow and vibrational energy. It is generally agreed that these energy sources have enormous potential for



supplying electricity to equipment used for energy collection. The main emphasis of the dissertation under consideration is on small- or micro-scale energy as shown in Fig. 1.

Fig 1: Categorization of sources of renewable energy

1.1 Piezoelectricity: An overview

In a nutshell, a piezoelectric material responds to external pressure or force by deforming by generating an electric charge. The piezoelectric material was first found by the Curie brothers [8]. Their study was restricted to the direct piezoelectric effect (Fig. 2), which is when a piezoelectric material is deformed and produces an electric current. Another French scientist discovered the "inverse piezoelectric effect" (Fig. 2), which results in the piezoelectric material deforming when exposed to an external electric charge. For their work, they studied the quartz crystals found in nature. They concluded that the generation of electric current from naturally occurring piezoelectric material is mostly caused by the growth of natural dipoles within the piezoelectric material. This fundamental phenomenon affects all currently utilized piezo-materials. Different positive and negative charge formations take place depending on the particular group of the piezo material [9].

The piezoelectric material is electrically neutral in the absence of tension and deformation, meaning that its positive and negative electrodes are in sync. The positive and negative electrode centers stretch or contract when the filament is under tension or pressure, creating a voltage difference and a field of current within the material. Fig. 2 (b). The conductive wire is connected to the positive and negative electrodes of the substance in order to transfer charge from it to the external circuit. The direct piezoelectric action of the piezoelectric material is based on this.

Contrary to what is assumed, a piezoelectric material's neutral behavior is influenced by an externally supplied electric field. The electric field will cause changes in the internal electrical dynamics of the piezoelectric material. In order to return the piezoelectric material to its original position and neutrality, the positive and negative electrodes must be moved in a way that allows them to resume their initial neutral locations. An inverse piezo effect is created as a result of the material being mechanically deformed and stress being added to the system.

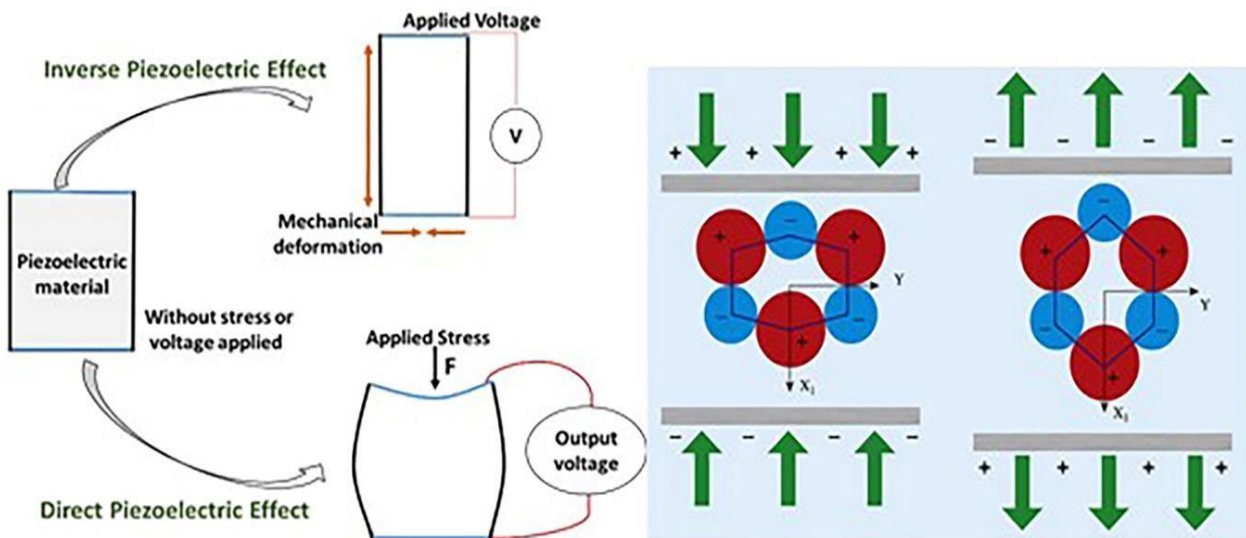


Fig. 2: (a) Inverse and direct piezo effect (b) Cell structure of piezo film

Following are more categories for piezoelectric materials:

1.1.1 Quartz

The ability of the quartz to change its shape is limited by its crystalline structure or other crystalline features. In addition to being stiff and having a low susceptibility to temperature and environmental factors, it also boasts strong piezoelectric capabilities. In frequency control modules, electronic watches, and other microprocessor-based devices, these are employed where greater precision is needed. In situations when a considerable degree of deformation is required, they are less suitable for utilization.

1.1.2 Ceramics

In spite of their extreme brittleness and limited applicability, ceramics have exceptional piezoelectric characteristics. The main advantage of this kind of material is that it is available in powder form, allowing it to be molded into a variety of shapes, including discs, cylinders, plates, and thin films. Although quartz has more durable piezoelectric properties than ceramics, it is nevertheless thought that this type of piezo material should be chosen because of its ability to conform to any shape.

1.1.3 Polymers

The most often utilised piezo polymer is polyvinylidene fluoride (PVDF). In comparison to quartz and ceramics, polymers are softer and more flexible in their natural state. They are used in many applications despite having poor piezoelectric qualities because of their flexibility.

The elasticity of them makes them more mechanically stable. Typically, they take the shape of thin filaments that can be stretched to the necessary length. They are frequently used in experimental research work pertaining to piezoelectric material energy generation because of the 4 abilities to endure massive deformations.

1.1.4 Composite materials

The rigidity of ceramics and the flexibility of polymers are combined in a unique sort of piezoelectric material that is soft and flexible while also possessing a specific degree of rigidity. The composite piezoelectric material can be utilised in research where substantial deformation is necessary because of these structural characteristics.

1.2 Reasons for choosing PVDF Flag

The following factors motivate the choice of the piezoelectric flag for energy harvesting

- It is adaptable enough to change and modify itself in response to impinging vortices produced by the bluff body in accordance with the Karman Vortex Street design.
- It exhibits motion with a high flapping frequency and a huge amplitude, which is consistent with the dynamics of a fluttering flag.

This type of piezoelectric flag flapping implies a continuous energy exchange between the piezoelectric flag and the surrounding fluid. Numerous researchers have been drawn to this energy exchange mechanism and are searching for new ways to harvest energy from it. Typically, energy extraction utilising flag-based energy harvesters may use one of two methods:

- either producing energy from the displacement of the flag [10]
- or from its deformation [11,12].

Some investigations using active piezoelectric material have lately been driven by the second method [13–15]. The current study chose the piezo material because of its flexibility and ability to convert a portion of mechanical energy, in the form of strain energy produced by fluid-structure interaction and flag deformation similar to a cantilever beam, into electrical energy.

1.3 Motivation

Scientists have come up with new methods and devised new strategies to successfully extract the sustainable energy from the other 5 natural resources as a result of the limitations of fossil fuels, the human race's dependence on energy-driven technologies, and the environmental impact of fossil fuels. Among the sources of obtaining renewable energy are

wind turbines, hydroelectric plants, and wave motion energy extraction. Researchers have been able to create novel, efficient, low-cost energy generation techniques because to recent advances in fluid-structure interaction research and the development of some smart materials. Small, unattended sensor packages require power generation and harvesting in order to carry out long-duration military missions and structural health monitoring. The monitoring of the building is important since it enables the early repair of any damage, which saves money on any catastrophic damage that can result from postponed repairs. Due to a number of considerations, power-efficient devices, such as microelectromechanical systems, are now being developed for use in the field and as a method of communication. A basic MEMS system includes a wireless communication system, a smart sensor, data transfer, and signal processing system monitoring. A strong power source is needed for each of these components. The need to continuously power MEMS and other self-sufficient devices led to the development of energy harvesting research. Providing batteries or a power line to assure a constant flow of electricity is the traditional way to power such gadgets.

However, these systems have several drawbacks, such as the necessity for routine battery replacement and the environmental problems brought on by the disposal of used batteries. The placement of the MEMS devices presents an additional difficulty for powering these systems. Reaching MEMS devices for battery change can be a very difficult process because the majority of them are located in hard-to-reach places. Given these difficulties, it would be perfect if we could locate the energy source exactly where it was required.

1.4 Research Aim

This study aims to “investigate the effect of boundary layer thickness by varying distance between side walls on piezoelectric energy harvester output”.

1.5 Research Objectives/Limitations

1.5.1 Objectives

The study is done on multiple fronts, and its primary goals are as follows:

- To study the effect of boundary layer thickness due to side walls of different width on energy harvesting
- To find the optimum position of the cylinder and eel at which we can obtain highest energy in terms of boundary layer thickness.
- To compare the results between different configurations for higher power output

- To obtain PIV results to analyze the fluid flow
- To make comparison of current study with literature results for two different bluff bodies configurations and understanding the difference between the results.

1.5.2 Limitations

This study has a few drawbacks that are described below; they could be addressed in subsequent research,

- The study was concentrated on energy harvesting; hence a thorough investigation of hydrodynamic forces must be done as it was outside the purview of this investigation.
- The study does not compare PIV wake flows with simulation data in order to evaluate two methods specifically for cut angles because it is an experimental study and simulation at high Reynolds numbers requires separate specialised equipment.

1.6 Structure of thesis

The thesis is divided into five chapters, each of which begins with a brief introduction criticising the objectives of the relevant material and concludes with a summary that highlights the key conclusions. Following is a breakdown of the thesis.

The theoretical underpinnings of the energy harvesting devices based on flow-induced vibration are covered in **Chapter 2**. Additionally, it describes how using nanomaterials like PVDF can increase its efficiency. It also provides an overview of the VIV phenomena, the theoretical basis for energy harvesting based on this phenomenon, and improvements in energy efficiency through bluff body form changes.

The study approach is thoroughly covered in **Chapter 3**. Here is a description of all the variables and tools used to conduct the experiment. It also goes through the methods employed for post-processing and analysis of the experimental data.

Chapter 4 covers the discussion of experimental results to study the impact of boundary layer thickness on energy harvesting by changing the both the streamwise and spanwise gaps along with plots.

Chapter 5 discusses the overall results of the thesis, summarises the key contributions to the work, and offers some perspectives and suggestions for additional research. Following it are references.

CHAPTER 2

LITERATURE REVIEW

2.1 Introduction

Self-powered instruments, also known as energy harvesting devices, are becoming more widely used to harness renewable energy sources from the environment. These systems, such as wireless sensor networks, are designed to be environmentally friendly and have seen considerable development in recent years [16,17]. The goal of utilizing naturally existing energy sources is to replace the conventional sources and create environmentally friendly energy options. The growing concern over the depletion of natural resources and the impact it has on human health and the environment has made renewable energy harvesting a widely researched topic [18,19].

Energy harvesting using piezoelectric materials have become a subject of interest for their potential use in applications such as wearable electronics, strain gauges and Internet of Things (IoT) [20]. Therefore, research into small-scale energy harvesting techniques is highly sought after as it can provide an efficient means of powering small portable gadgets like surveillance recorders, self-power supplies, application in pathways, stopwatch, MacBooks, temperature sensors, micro/nano robots, UAV's, and similar equipment of daily use [21–27]. For example, a nano-robot is a highly sophisticated device capable of detecting and adapting to its surroundings, manipulating various objects, and executing complex tasks. One of the key challenges to be tackled is finding a self-sustaining energy source that can power nano-robots without compromising its functionality [28–30]. The use of alternative micro-power generators utilizing flexible flags in vortex vibration environments can provide a suitable replacement for traditional disposable batteries in the field of electronics [31]. The use of vibration-based energy harvesting, a method of converting fluid motion energy from vibrations into self-sustaining power, has risen with the advancement of micro-electronics, miniature sensor technology in the past two decades. Piezoelectric Vortex Induced Vibration (VIV) based transduction, one of the approaches to harness the flowing fluid energy, is a prevalent strategy for mechanical to electrical energy transformation [32,33]. The piezoelectric energy harvester, with its basic design and superior performance, holds great promise and is currently being explored for its potential uses and limitations. Further, one of its standout characteristics is itself usage as sensor node [34,35]. The shedding of regular eddies in the downstream area of a bluff body because of fluid interaction and pressure variation triggers the onset of VIV [36].

A piezoelectric flag made from PVDF can be strategically positioned to effectively capture energy from the surrounding environment [37]. The PZT patch can generate more energy due to its high dielectric constant [38], but it has limitations and cannot handle large amplitude [39]. Moreover, the choice of PVDF flags has got separate significance in this regard only due to factor of high execution under harsh conditions, especially, in more windy scenarios [40]. Allen and Smit [11] proposed a method of harnessing energy from flowing fluid using flexible flags (piezoelectric eel). These flags, when exposed to wake flow, vibrate like beam immovable at one end with significant amplitude and frequency, allowing for the conversion of kinetic energy of flowing stream into electrical power.

2.2 Energy harvesting using FIV technique

Fluid flow-induced vibrations have emerged as a highly promising method for autonomous power generation, providing an independent energy source for micro-devices without reliance on external power supplies [41]. A boundary layer is formed at the interface of moving flow stream and bluff body [42,43]. When the boundary layer detaches from the wall, a distinctive vortex formation result. Further, the von Karman vortices forms because of the flow patterns being shed from the resistance blunt body [44]. Wang et al. [45] in his study investigated into different frameworks and strategies to extract energy due to Flow Induced Vibrations (FIV) phenomena. The strain produced by the movement of the shed vortices leads to the generation of electrical power when the piezoelectric flag begins to flutter [46–48]. Williamson [36] presented a comprehensive examination of the mechanics behind the vortex formation and dissipation in the wake of circular bluff body, from the emergence of shear film to the eventual dampening of the vortex. The downstream flexible body can harness this vortex shedding to enhance its propulsion and flapping capabilities while reducing drag [49]. Numerical and parametric studies have been carried out to explore the potential of capturing energy from vibrations caused by vortices in a marine ecosystem [11,50–53].

Gkoumas et al. [54] applied multiple approaches to investigate the energy scavenging possibilities of flexible eels in aquatic environment. The findings revealed how the fluid dynamics in the ocean work in conjunction with the flexible flag, altering its shape to match the wake of a cylinder that is not hindered. Dung et al. [55] practiced novel method utilizing the synergistic interaction of electromagnetic induction and vibration brought on by vortices, to generate power output from motion energy of flowing fluid. The results reported the instantaneous power, depicted as P_{ins} of $1.77 \mu\text{W}$ when subjected to a fluctuating force with a frequency of 62 Hz. Mehedi et al. [56] performed a computational investigation of varying

fluid flow characteristics on a flexible flag situated within a narrow fluid channel. Shi et al [57] analyzed the impact of the aspect ratio on the effectiveness of energy harvesting through experimentation. To optimize energy harvesting performance, bluff bodies with various geometrical shapes were employed and an improvement of 26.5% and 45.7% in efficiency was reported. Usman et al. [35] evaluated the impacts of an asymmetric wake flow regime on the electrical energy output for two cylindrical bluff bodies placed side by side using cantilevered flag. The results demonstrated an increase of 95% in harvesting energy when the distance between two cylinders (N/d) was observed one.

2.3 Energy harvesting in Tandem configuration

Several studies have been conducted by different researchers, utilizing the tandem configuration, to demonstrate the interaction dynamics, fluid drag and pressure gradients to amplify the overall performance of the system to for energy scavenging [58,59]. Fuwang et al. [60] performed the experimentation setting passive piezoelectric flag in tandem arrangement at tandem distance-based Reynold number ($Re = \rho Vd/\mu$) of 8.7×10^4 , which reported 19.6% boost in energy efficiency when chord length was one. Zhang et al. [58] proposed the implementation of a cylinder with dissimilar profiles and noticed a significant increase of 380% in performance upon integrating bluff bodies. Mujtaba et al. [61] also conducted experimentation to investigate the behavior of rear and front cantilever beams in tandem arrangement, which reported more drag and power on rear flag at streamwise distance of 1.75 m at a water speed of 0.26 m/s from VFD. Further, the setup showed the boost of 116% in output power due to strain generation in flexible flag. Xiaobiao et al. [62] assessed the capacity of microfiber composite's piezoelectric energy harnessing and stressed the influence of harvester spacing and flow stream velocity employing two cylindrical bluff bodies aligned in tandem design.

The dynamic forces of a moving fluid can enhance the piezoelectric beam's transitory deformations by integrating a cylinder at the free end. Additionally, the harvester moves as a result of the fluid's uneven pressure distribution, putting strain on it. Hu et al. [63] performed experimentation to demonstrate how adding little rods at different angles around the diameter of a circular cylinder can increase performance. The unstable region expands as a result of this adjustment, which reported increase in power output. Usman et al. [64] carried out experimentation to study the impact of an inverted C shaped bluff body with different cut angles. The study reveals that inverted C type cylinder with 120° gains maximum power of 66% in comparison to circular cylinder. Wang et al. [65] anchored two Y-shaped foils to the

surface of a cylindrical object, demonstrated the phenomenon of converting VIV into galloping. The analysis proposed 60° inclination angle to maximize performance and increase turbulence. The change in the shape of vortex generating body (bluff body) resulted in a large boost in power output. The rippling flag displays flutter, and beyond a critical velocity, it transitions into limit cycle oscillations leading to high amplitude movements. Consequently, energy is harvested at a low or constant frequency through wide amplitudes [66,67]. A computational study was carried out to investigate the effect of underwater depth, in the wake of circular bluff body, using VIV. The results depicted sharp increase in power hydro-power when the depth increases from 0.1 m to 0.5 m [68]. The dynamic forces of fluid flow can amplify strain in the piezo beam by attaching a cylinder at its free end, causing an unbalanced pressure distribution, leading to more movement and strain production within the flag [69–74].

2.4 Geometrical shapes

Numerous research studies have been undertaken to refine the geometrical configuration of bluff bodies in order to maximize the efficiency of piezoelectric films. The T-shaped bluff body was first tested in wind tunnel for shape change, yielding 4.0 mW power at 4.0 m/s wind speed [75]. Through computational and experimental investigations, studies of the voltage output from a three-blade bluff body showed that maximal voltage occurred when the half-angle of blade was adjusted between 60 and 80 degrees [76]. The energy-harvesting performance of four-cylindrical shapes were investigated by Ding et al. [77] over a Re range of 10,000 to 130,000, revealing highest output at Re = 60,000 for q-trapezoid shape. In other studies which have been done so far, a bluff body was utilized as end mass to induce galloping, strengthen the capability of energy harvesting together with synchronizing the frequency at which vortex shed with natural frequency of flag to establish resonance transversely [78,79]. The impact of the cross-sectional design of a bluff body on energy scavenging from galloping phenomenon was investigated by Abdelkefi et al [80].

Sufficient research has been carried out regarding wake flow characteristics of single/multiple bluff bodies using piezoelectric cantilever beam, but limited research was conducted to portray the impact of boundary layer on power scavenging changing channel widths. Some researchers explored flow in different channels with regards to flow dynamics. Sun et al. [81] analyzed the response of triangular prism and cylinder in an open channel while using macro fiber composites glued to a cantilever beam to harvest energy. Moreover, the response of flexible flag was also analyzed at different flow velocities. Dellinger et al. [82] conducted study to demonstrate the trend for hydroelectric power in confined space. The outcome demonstrated

the dependency on inertial and peripheral conditions. Neo et al [83] used water channel to explore the impact on energy harvesting by fixing shape and speed of water droplet (triboelectric effect). The Teflon coated electrodes were installed at top and bottom of the channel, revealing closed circuit current of 2.346 ± 0.018 nA with thinnest layer of Teflon. Further, sharp increase in energy was noted with the increase of droplet speed. Goushcha et al. [84] examine the impact of different piezoelectric beams placed in different boundary layer regimes with Reynold number 2000 to 7500. Sun et al. [85] attached meta-surface with cantilever flag and changed the height for staggered and normally attached tri-prism arrangement to improve energy harnessing.

2.5 Novelty of this research

Previous studies have emphasized the crucial role that the shape of the bluff body and size variation of channels play in flow dynamics. However, no research has been conducted to comprehensively investigate the impact of channel size on energy harvesting by changing both streamwise and spanwise gaps. The phenomenon discussed in previous studies is either flow behavior in closed/open channels or simply energy harvesting using bluff bodies [86–88]. The impact of channel size variation on energy harvesting has not been studied yet. This study investigates the impact of boundary layer thickness on energy harvesting by varying the distance between side plates of an open channel, using two different bluff bodies for wake generation.

This study shows substantial merits of utilizing two different bluff bodies and different plate distances for improvement of wake dynamics to harness more energy. This investigation is crucial in developing practical and portable self-sustaining devices that can generate electrical energy from fluid flow, as it will provide insights into how to optimize the design and maximize the energy output of piezoelectric-based energy harvesters. Experimentation using Particle Image Velocimetry (PIV) is performed to assess the transformation of the wake and its impact on the output power as the flag oscillates at maximum amplitude behind the bluff body which is equal to the width of the wake [11]. Therefore, the out power is directly dependent on wake width. The circular cylinder and C-type inverted cylinder (120 cut angle) are used as bluff bodies as both are used in the past studies for energy scavenging [33,64]. However, no impact on energy harnessing is explored by changing the distance between plates using these cylindrical bodies. Streamwise gap is changed from 1 to 5, which fully covers the wake of bluff bodies to identify the optimal position to harvest maximum energy. Spanwise gap is changed from center towards boundary in terms of boundary layer thickness depending upon the width

of channel. This new method addresses prior limitations and issues, showing a novel energy harvesting concept suitable for use in tidal environments.

CHAPTER 3

EXPERIMENTAL METHODOLOGY

3.1 Water Tunnel Setup

The investigation employs a slow-speed water channel that operates in a closed loop system, as shown in Fig. 3 located in Department of Mechanical Engineering at National University of Sciences and Technology (NUST) [89]. The test area of the water channel is a square configuration with dimensions of $2000 \times 400 \times 400$ mm ($L \times W \times H$). A variable frequency drive (VFD) ranging from 1 to 50 Hz is used to regulate the RPM of the centrifugal pump, which drives the water tunnel. This allows for the water velocity adjustment in the range of 0.1 to 0.5 m/s measured using Particle Image Velocimetry (PIV) technique, having a turbulence intensity not exceeding 1% at maximum. The flexible eels made of polyvinylidene fluoride (PVDF DT2-052K/L with rivets, manufactured by Measurement Specialties Inc., P/N: 2-1003744-0) are held in place at the leading edge by thin steel rods with a diameter of 4 mm. These flags are attached to the rods and fixed in place over the walls of the test section using a clamping fixture. The illustration in Fig. 4 display the schematic of the setup and Fig. 5(a) and (b) presents a schematic representation of the placement of both bluff bodies and the cantilever flag.

The flow is made uniform through the use of aluminium honeycombs with hexagonal openings, measuring $1.83 \times 0.5 \times 0.0254$ m ($L \times W \times H$). The effect of boundary layer on enhancement in energy scavenging using flexible eel is investigated by varying the distance between side walls/boundaries. The three different widths with dimensions 360 mm, 310 mm and 260 mm are utilized. The circular and 120 C-cut inverted cylinders are used as bluff bodies to set up wake. The highest blockage ratio measured, in case of minimum width (260 mm), is 9.61%, which falls within the acceptable range as investigated by Choi et al [90]. The bluff bodies and piezoelectric flag are rigidly attached to the traverse on the top to avoid any lateral motion or vibration.

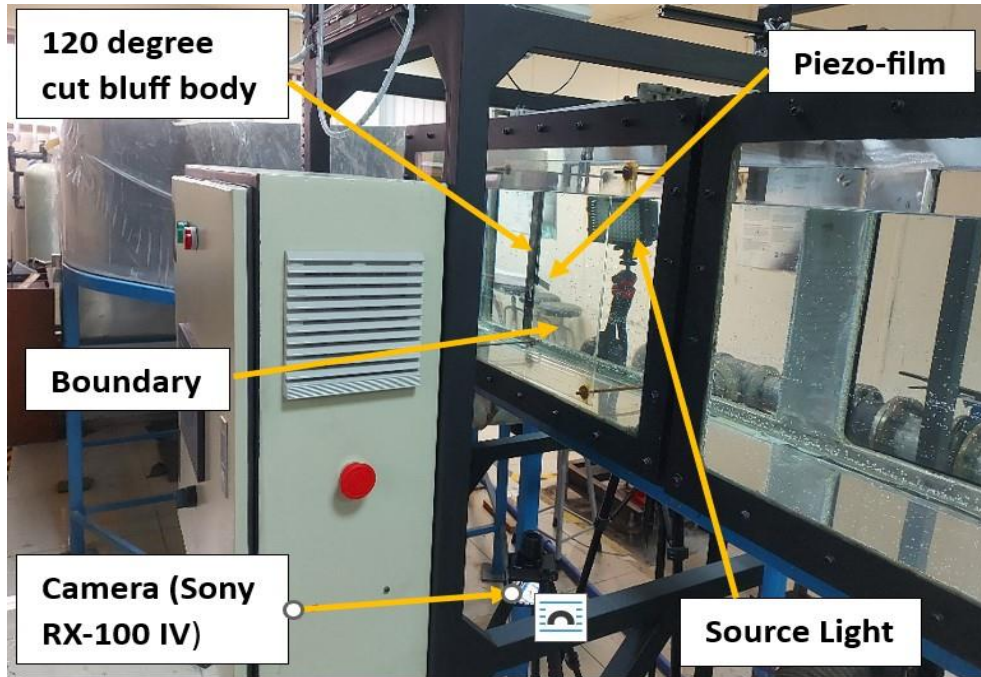


Fig. 3: Real Time experimental setup of water channel

The experimental setup for this study includes flexible eel, mainstream velocity, high resolution camera, a breadboard equipped with a suitable resistor for load circuit, and a DAQ, a device to record instant voltage generated in flexible film due to strain. The accuracy of the DAQ card is verified by comparing output voltages taken under similar conditions using a digital oscilloscope (UTD-2052CL), and the found the results are the same. The PVDF flag is 0.072 m long and 0.016 m wide, but its active length is only 0.060 m since the connections are insulated using epoxy gel and sticky tape. The choice of this flag/material is made based on its mechanical adaptability and ability to endure substantial deformation compared to ceramic piezo material (PZT). The flexible flags can generate power up to 100 V depending upon magnitude of strain applied and load resistance of the circuit. The cantilevered flag is shown in Fig. 6 and its properties are shown in Table 1. The spanwise gap is varied in terms of boundary layer thickness with constant gaps for each width.

Two LED lights are used to shed light on the experimental section. To counter the influence of light interference, the area under testing was housed with dark cloth. A high-speed camera (Sony RX-100 IV) is used to record the flapping of flag. The video of each experiment is recorded for 2 min at a rate of 50 frames/second for high resolution. Video data is post-processed using MATLAB code to record the trace of flapping frequency, amplitude, and normalized frequency of the flag. The code keeps track of the flag's fluttering movement, creating a comprehensive excel file that automatically records instantaneous data, including

position and time. The complete details of parameters for experimental setup are shown in Table 2. The maximum amplitude (A/L) for piezoelectric film is determined by tracing the area it covers while fluttering under forced conditions using MATLAB code. Further, FFT analysis is performed on excel data to determine the dominant normalized frequency.

The turbulence intensity in the current investigation stands at less than 1%, revealing the laminar flow and the reliability of the experimental results and data collected. This is recorded by regulating the flow velocity through variable frequency drive (VFD) using the formula:

$$TI = \frac{a'}{A}$$

where, a' denotes the RMS (root mean square) value of the velocity fluctuations and A denotes the mean flow velocity.

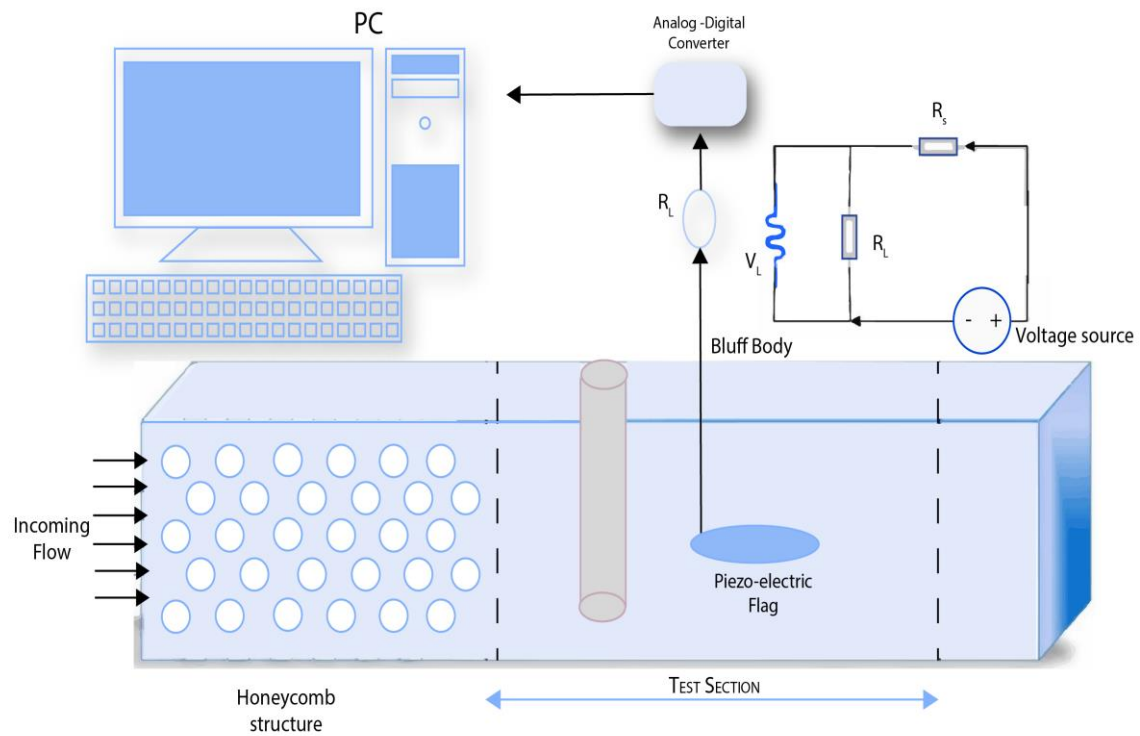


Fig. 4: Schematic of complete experimental setup

Table 1

Physical traits of flexible energy harvester and its material

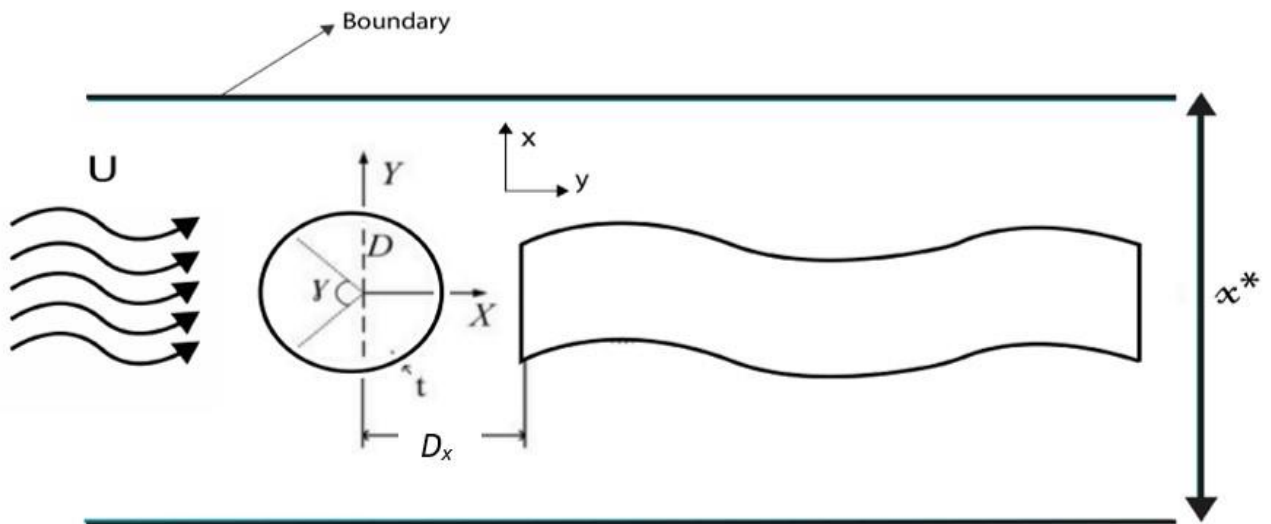
Parameter	Value
Total length of flag (m)	0.072
Active length of flag (m)	0.060
Width of flag (m)	0.016
Flag's material	PVDF
Output voltage range (V)	0.01-100
Flag's Youngs modulus (10^9 N/m ²)	2-4
Operation temperature (°C)	0-70
Capacitance of flag (pF/cm ²)	1.44
Density of flag material (kg/m ³)	1.78
Relative permittivity (ϵ/ϵ_0)	12

Table 2

Setup parameters details

Parameter	Value
Fluid	Water
Density of fluid (kg/m ³)	998
Fluid temperature (°C)	25
Diameters of cylinder (m)	0.025
Number of cylinders	2
Thickness of cylinder (t) (mm)	1.5
C-section cylinder cut angle (γ)	120°
Cross section of second cylinder	Circular
Diameter of rod (mm)	4
Rod and cylinder material	Aluminium
$D_x = d_x/D$	1-5
$D_y = d_y/\delta$ (plates distance dependent)	9.48-52.89 (from cylinder centre)
Distance's range between plates (mm)	260-360
Blockage ratio	(6.94-9.61)%
Velocity (m/sec)	Constant
Seed particles for PIV	Hollow glass spheres
Material mean composition (μm)	15
Density (kg/m ³)	1050
Refractive index	1.5

(a)



(b)

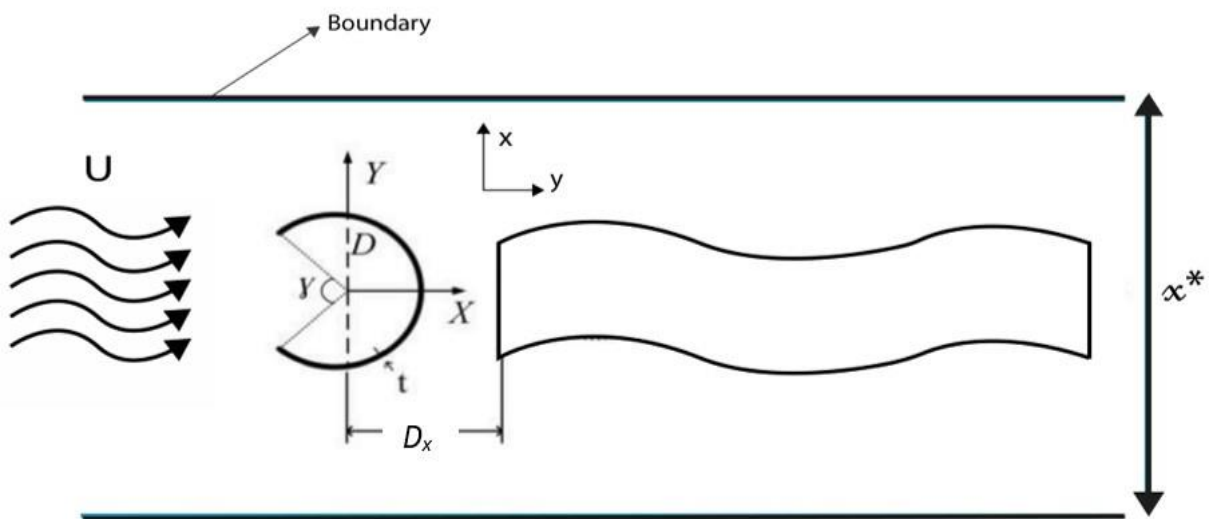


Fig. 5: A schematic of the experimental setup is depicted, showing a flag that is clamped at its leading end and free at its trailing end (top view) (a) Circular cylinder (b) 120 degree cut C-type inverted cylinder.

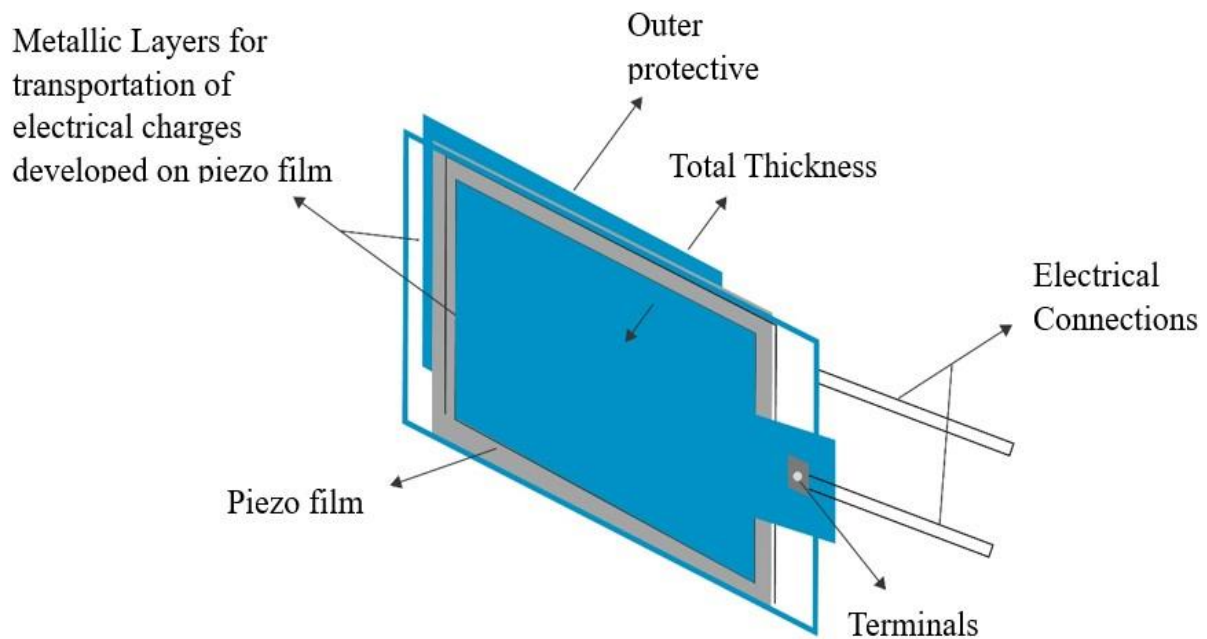


Fig. 6: Details of cantilevered flag

3.2 Particle image Velocimetry

The incredible science of particle image velocimetry uses tracer particles to create an image that explains the flow characteristics while employing an optical method to examine fluid structure and flow behaviour, notably in the wake zone. PIV is a flow visualisation method used to produce instantaneous fields of vectors (velocity) and scalar data, including fluid-related characteristics. The fundamental element of this arrangement is seeding particles because it is impossible to understand flow behaviour without them; therefore, one must essentially introduce them into the fluid that is moving. There are many different kinds of particles available on the market, depending on their intended application and the medium in which they will be utilised. For example, smoke is used when the fluid is air, while beads, dye, or hollow glass particles are used when the fluid is water as a tracer particle in the flow field. The density of the particles is quite similar to the fluid's density. To enable detection by the digital camera mounted beneath the test area, these particles are lighted using an optical laser 34 or pair, depending on the application. Using a cross-correlation technique, the sequential camera images of tracer particle motion are processed to obtain information about the flow field under study with respect to flow velocity (the direction of motion and speed of particles). Fig. 7 illustrates this method, which correlates two photos to determine the distance travelled

over time. Additionally, the analysis and processing of this data reveal details on flow or speed lines, flow vortices, and the distribution of view field characteristics. A typical particle image velocimetry setup consists of a digital CMOS/CCD camera, a laser with an optical setup to generate the physical light sheet to illuminate the desired/specified flow field, a synchronizer to control the timing of camera and laser triggering, the tracer particles, and the fluid being studied.

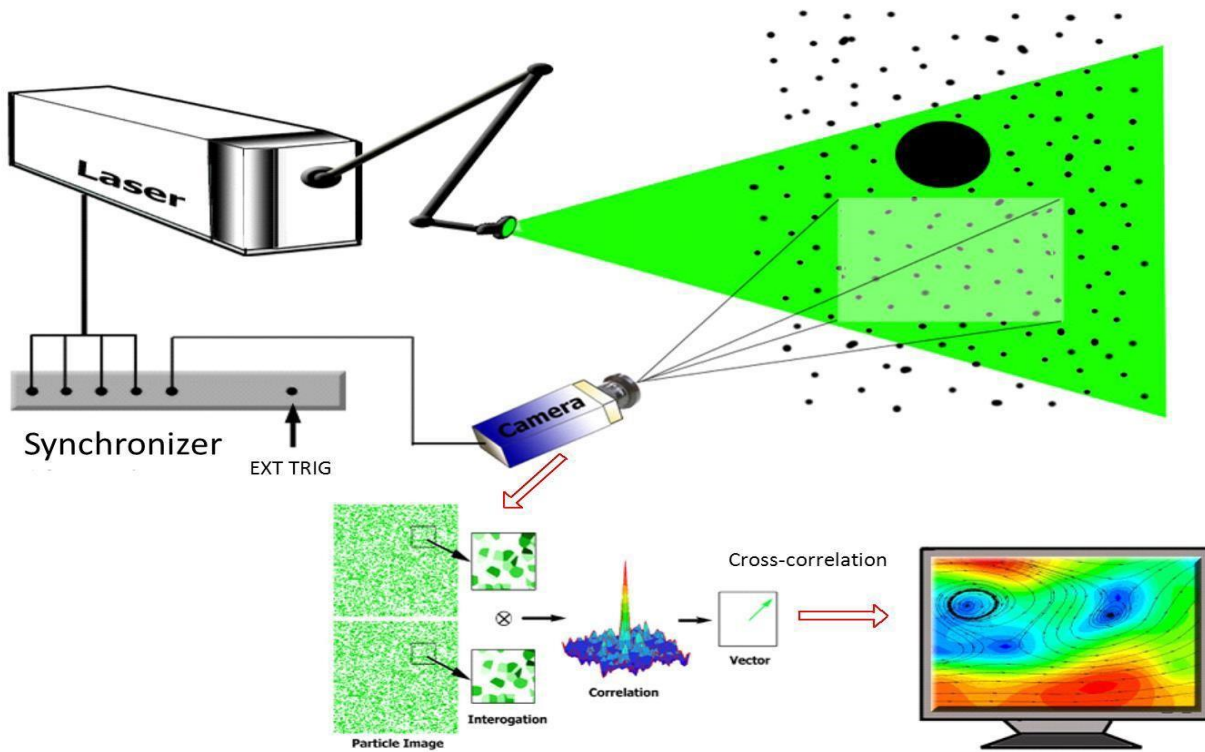


Fig. 7: Schematic for PIV System

An adjustable and fixed camera and laser setup with its lens, which turns the laser beam into a laser sheet, is made possible by a three-dimensional transverse mechanism. The optical pictures are post-processed using PIV MicroVec or another software option. The CCD camera needs at least two exposures of laser light from the flow field (with a known time interval t), while the tracer particles track the fluid path. Particles flowed in accordance with the flow, and two photos were captured with different positions. These images were recorded on the CCD chip and sent to a 35 PC. If we know that two groups of microparticles will move at the same time in t_1 and t_2 , we may use the speed of the definition equation to derive the particles' velocities at time t_1 using the particle picture recorded from the recording media, as shown in the equation below.

$$U = \lim_{\Delta t \rightarrow 0} \frac{\Delta S}{\Delta t}$$

PIV technology generally operates under three presumptions:

1. Tracer particles move with the flow of the fluid.
2. The flow field contains a homogenous distribution of tracer particles.
3. An interrogation window with a distinctive speed.

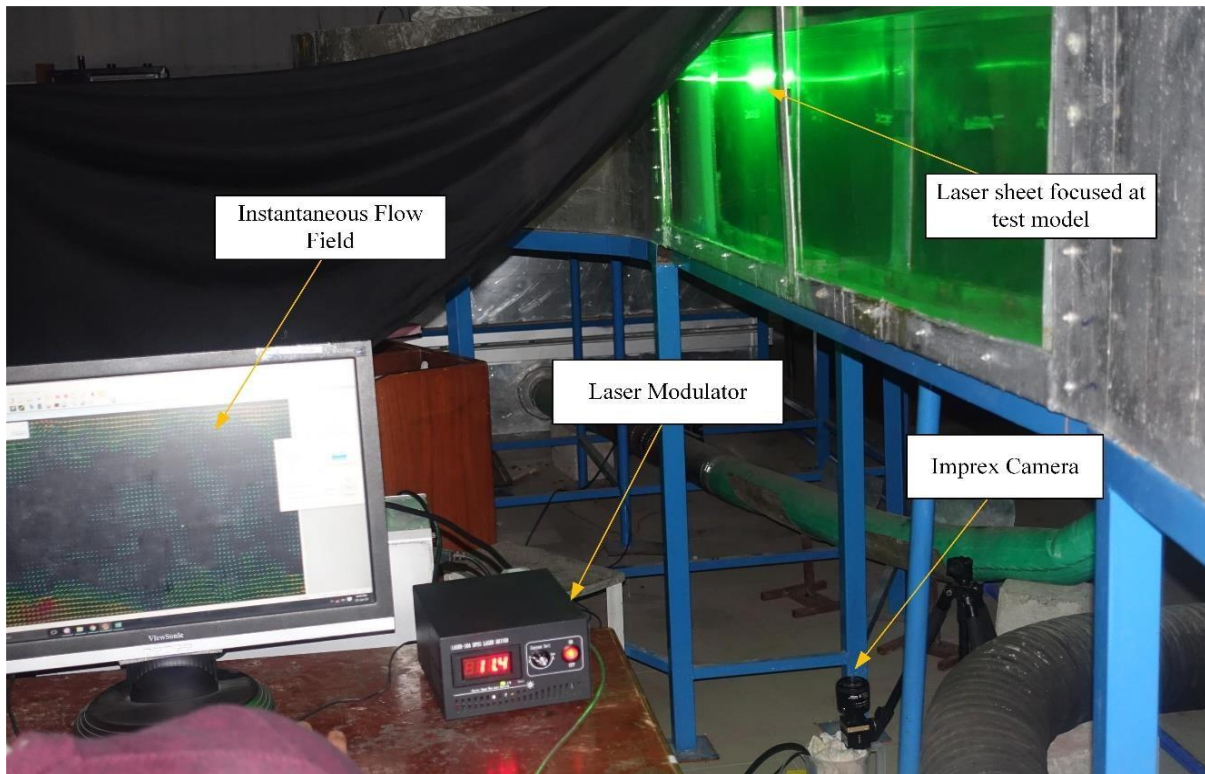


Fig. 8: Real time setup for PIV

In a region that has been illuminated by optical laser light, instant velocity vectors were calculated using the particle image velocimetry approach. Additionally, PIV investigations are carried out with the MicroVec PIV system, which uses a 5-Watt Diode pumped Solid-State (DPSS) laser with a 532 nm wavelength. Images as displayed in Fig. 8 were taken using a charged coupled device (CCD camera, Imprex CLB-B1320M) with a spatial resolution of 1280 pixels by 720 pixels and a maximum sampling frequency of the system of 30 fps. Throughout this study, unless otherwise stated, two 32 x 32 pixels square 36 influential windows are employed for image processing. The display speed is 10 f/sec, and the photos are captured at 30 fps. Before testing, the MicroVec professionals calibrated the apparatus.

The laser's frequency limit is set to 40, its laser threshold to 100, and the duration of both laser pulses to 200 s. The setting for pulse width is between 100 and 1000. A total of 4500 velocity

vectors were collected for an instantaneous vector field analysis. In this work, there was a 6-millisecond gap between each of the two subsequent laser sheet pulses that illuminated the measuring view field. After image processing, incorrect vectors were taken into consideration and improved using the interpolation approach among nearby vectors. Due to the PIV cam lense's visual limitations, larger cut angles require the overlap in order to cover the whole flow field.

Velocity vectors were calculated using the displacement vector area. The image's overall size was 1280 x 720, and 15 Hz was used to acquire patterns of instantaneous particle views (totaling 500 views). Tracer particles are hollow glass particles with a density of 1.05 g/m³. The "SM-MICROVEC3, 2D2C PIV/PTV software" (created by the World Technology Development Co., Ltd. in Beijing) uses the frame-to-frame cross-correlation technique to calculate the velocity vectors and integrates the PIV, PTV, concentration and particle size analysis, and field analysis module. The PIV MicroVec software-generated data files are further processed using the Tecplot programmes to obtain the swirl models of the wake. Using the velocity information, circulation and streamlines were gathered and plotted.

CHAPTER 4

RESULTS AND DISCUSSION

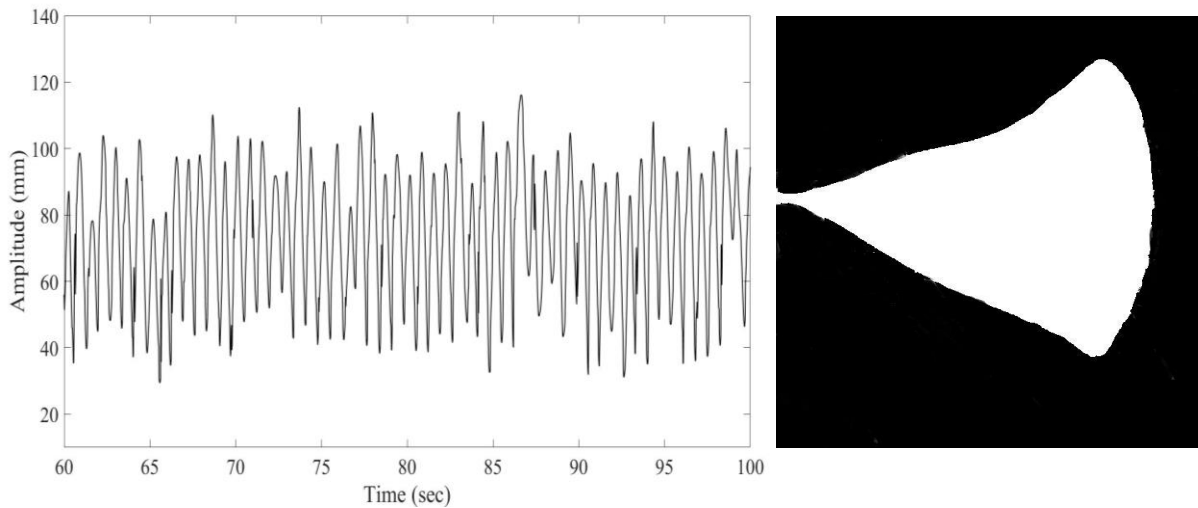
The optimal configuration of energy effectiveness of cantilevered flag positioned behind two different bluff bodies is found by varying the gap between plates, x^* , spanwise gap between cylindrical bluff body (each) and plate boundary in terms of Blasius boundary layer thickness (δ), D_y , and streamwise gap between trailing/clamped end of flag and centre of cylinders, D_x . This research investigates the impact of boundary layer thickness by changing streamwise/spanwise gaps and geometric parameters on the efficiency of the flexible flag, which utilizes an inverted C-shaped (120° cut) and solid circular bluff bodies. In general, the outcomes of the experiments indicate that changes to these parameters generate diverse modes of flapping, which in turn leads to better energy scavenging.

The flexible sheet, positioned in the wake of a cylinder, is inherently affected by the phenomenon of vortex shedding. This results in the flag being influenced by vortices shed from the upstream cylinder, leads to bending of flag and develops strain in the piezoelectric eel which in turn creates an electric charge in the flag. Strain produced in flag can be found by utilizing the beam theory of shapes. It demonstrates that the energy extracted by the piezoelectric film depends on several factors including maximum amplitude, capacitance of piezo film, normalized flapping frequency and thickness of flag [11]. As stated by previous investigation [91] that generation of electric charges and deformation in piezoelectric eel are directly related. By leveraging the same principle of power generation and deformation, power generated, and optimal tail position are experimentally investigated. During the experiments, different flapping modes of a flexible flag, such as continuous, periodic, and biased, are observed. The average power generated is computed using the relation $P = V_{rms}^2/I$ where V_{rms} root mean square value of instantaneous voltages recorded in 2 minutes time span using DAQ and I is the external load resistance of circuit calculated using maximum power transfer theorem. The evolutionary trajectory of the tail position, along with the corresponding envelope plots for both highest and lowest energy configuration are shown the Fig. 9(a) & 9(b), respectively. It is clear from the literature that a maximum amplitude equivalent to the width of the wake can be achieved by a flag positioned within the wake region of a bluff body [11]. Hence, an increase in wake width will lead to a higher oscillation amplitude. Similar trends are found in this study, as illustrated in Fig. 9(a), and can be attributed to the configuration that generates the maximum

energy. Whereas Fig. 9(b) represents the configuration that generates the lowest energy among all configurations tested in this study.

The detailed results of each cylinder, distance between piezo film and bluff body (D_x), gap between two side wall boundaries (x^*) and gap between cylindrical bluff body and plate boundary (D_y) in terms of boundary layer thickness (δ) are studied and discussed in depth in the following sections.

(a)



(b)

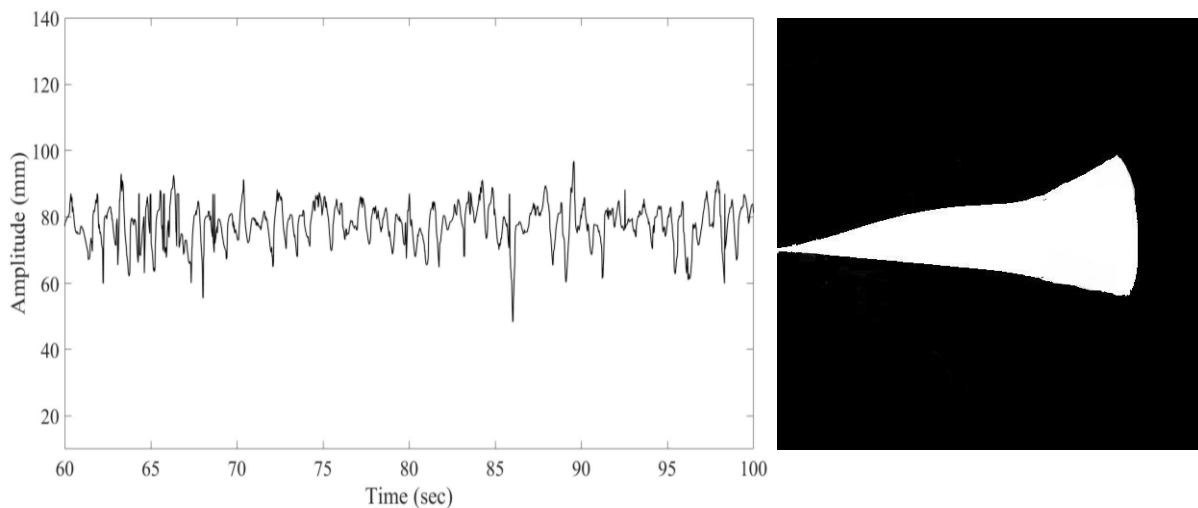


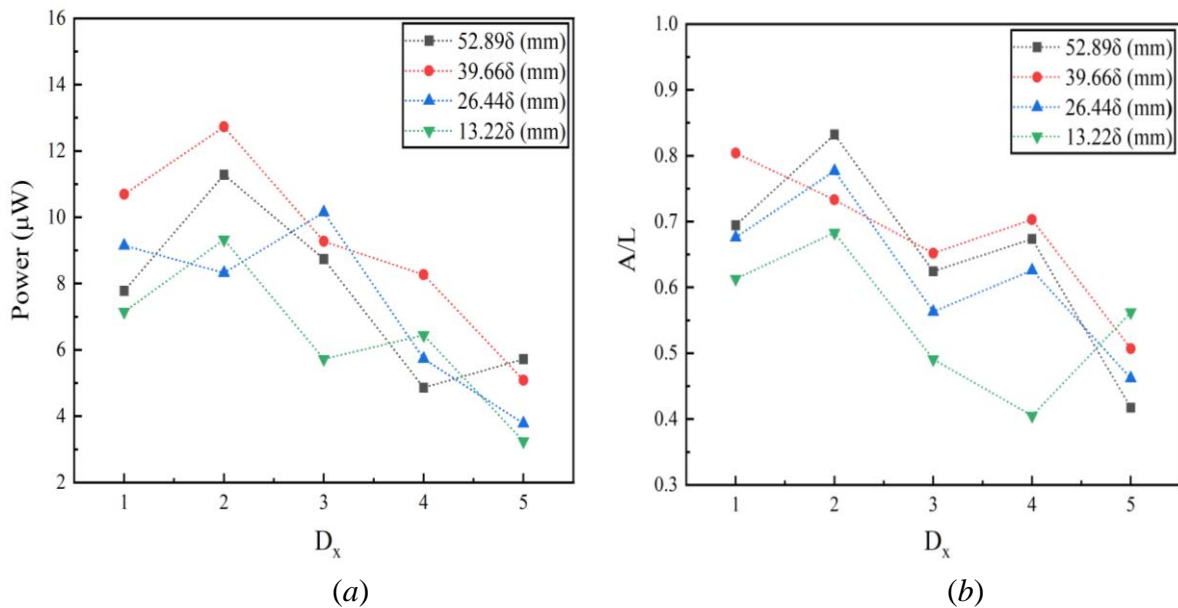
Fig. 9: (a) Variation of Non-dimensional peak amplitude and flapping envelope for high energy output configuration at $D_x = 3$ and $D_y = 34.05\delta$ (b) Variation of Non-dimensional peak amplitude and flapping envelope for high energy output configuration at $D_x = 5$ and $D_y = 18.96\delta$

4.1 Performance and Response of harvester for different geometrical cross sections

4.1.1 Experimental Measurements using circular cylinder as bluff body at distance of 360 mm between plates

Fig. 10(a) shows the maximum power obtained using flexible beam placed in the wake of the circular cylinder, which is considered as the benchmark case in comparison to 120o cut C-type inverted cylinder to validate the literature results. The highest power harnessed is for streamwise gap between $D_x = 1.0-2.0$ and spanwise gap between $D_y = (39.66-52.89)\delta$ at constant flow velocity of $U = 0.35$ m/s. The minimum levels of harvested power are witnessed for higher gaps ($D_x \geq 3$). To comprehend this behaviour the trend lines for maximum amplitudes and dominant frequency are shown in Fig. 10(b) and (c) respectively.

The decrease in harvested power output beyond the gap distance of $D_x = 2$ is attributed to the reduction in both flapping amplitude and oscillating frequency of the piezo flag. This reduction is due to the increased distance between the bluff body and the fluttering flag, which negatively impacts the performance of energy harvester. The maximum power obtained for this configuration is shown in Fig. 9(a) at $D_x = 2$ and $D_y = 39.66\delta$. Likewise, the point minimum harnessed energy is given as $D_x = 5$ and $D_y = 13.22\delta$. Based on the results presented in Fig. 10(b) and (c), it is apparent that the highest levels of flapping frequency and amplitude are associated with the point of maximum energy generation. The maximum amplitude (A/L) recorded for the circular cylinder is 0.88 for maximum power configuration at a slightly higher velocity, which is in good agreement with literature [92].



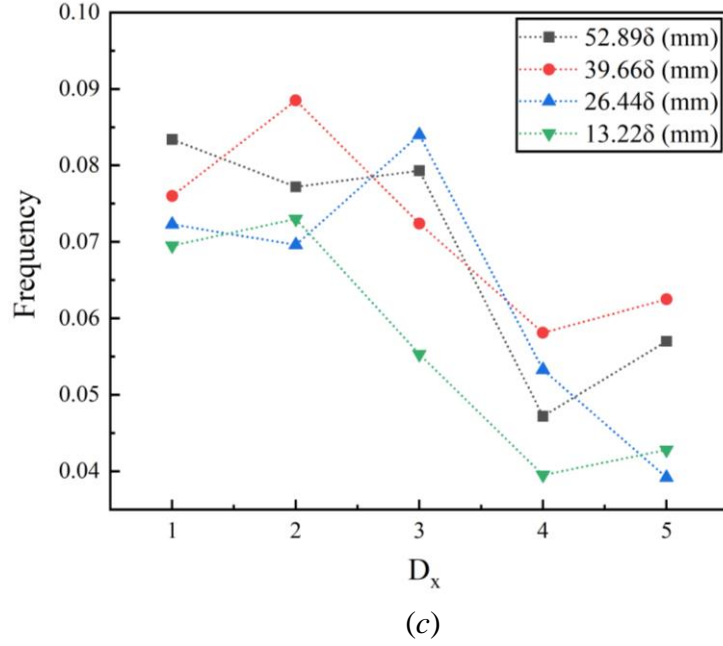


Fig. 10: (a) Power output (b) non-dimensional flapping amplitude (c) dominant frequency for circular cylinder for streamwise gaps ($D_x = 1-5$) and spanwise gaps ($13.22 \leq D_y / \delta \leq 52.89$) for $x^* = 360$ mm at constant velocity.

4.1.2 Experimental Measurements using 120 degree cut C-type cylinder as bluff body at distance of 360 mm between plates

Fig. 11(a-c) displays the acquired results for the power output, peak amplitude, and dominant frequency of a 120° cut C-type inverted cylinder. Analyzing the plots depicted in Fig. 11(a), the point of highest energy is at $D_x = 3$ & $D_y = 39.66\delta$ as the Fig. 11(b) & 11(c) clearly indicating the maximum flapping amplitude and dominant normalized frequency respectively, at the same streamwise gap ($D_x = 3$). In comparison to circular cylinder, the 120° cut cylinder exhibits the highest peak to peak amplitude due to strong coupling between wake of bluff body and flapping flag. High value of normalized frequency and bi-directional curvature results in more energy scavenging which is consistent with the existing literature that more peak to peak movement (A/L) and flapping frequency affirms more power output. However, as shown in Fig. 11, as the streamwise gap (D_x) between the 120° C-shape cylinder and the cantilever flag increases beyond $D_x = 3$ and spanwise gap ($26.44 \leq \delta \leq 52.89$) between cylinder and wall boundary is changed, there is a decrease in non-dimensional peak amplitude, power output, and normalized frequency, indicating the existence of a critical point beyond the specified value. At $D_y = 39.66\delta$, the movement of flexible flag is asymmetric results in more strain in one direction, results in more power output. For closest gap to wall ($D_y = 13.22\delta$), the energy harvesting in start is more for smaller streamwise gaps but decreases for $D_x \geq 2$ because more energy is utilized to overcome fluid's viscous effects due to boundary layer thickness (δ) [93]. Moreover,

the movement of flexible eel is also restricted close to boundary and streamwise oscillations and vorticity wavelengths also get reduced results in low energy generation.

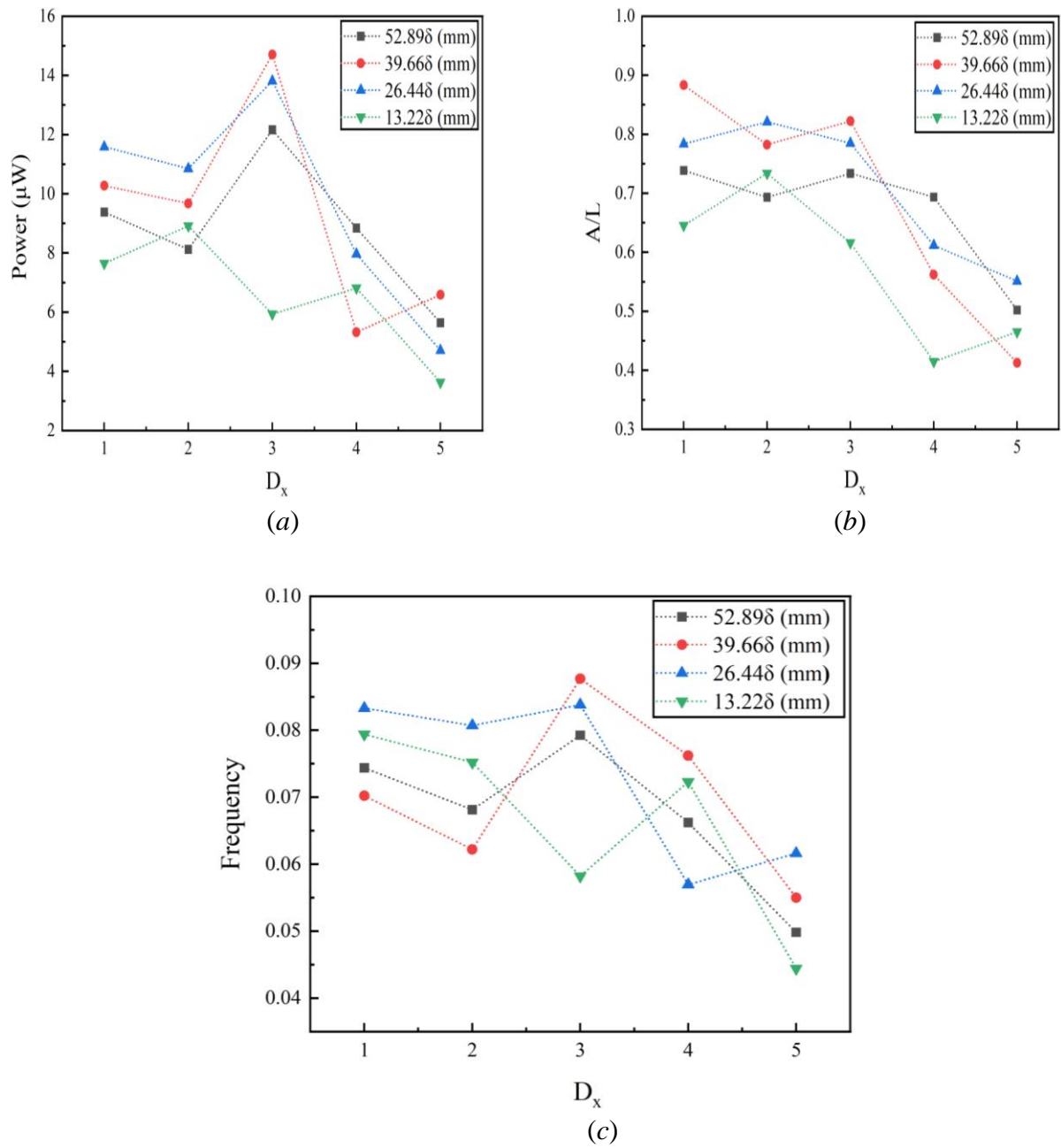


Fig. 11: (a) Power out (b) non-dimensional flapping amplitude (c) dominant frequency for 120° cut inverted C-type cylinder for streamwise gaps ($D_x = 1-5$) and spanwise gaps ($13.22 \leq D_y/\delta \leq 52.89$) for $x^* = 360$ mm at constant velocity.

4.1.3 Experimental Measurements using circular cylinder as bluff body at distance of 310 mm between plates

The plots of peak-to-peak amplitude normalized dominant frequency and power output for circular cylinder versus D_x against different values of D_y ($11.35 \leq D_y/\delta \leq 45.41$) are shown in Fig. 12. The distance between the side boundaries is 310 mm for the current case which is less than the aforementioned case to properly cater the effect of boundary layer thickness on energy harvesting. It is clear from Fig. 12 that for $1 \leq D_x \leq 5$ and $11.35 \leq D_y/\delta \leq 45.41$, the value of A/L varies from 0.33 to 0.86. However, the case with $D_y = 22.70\delta$ and $D_x = 2$ has more value of peak amplitude in comparison to all other cases. Due to the asymmetric movement near the wall, the piezoelectric cells experience more stresses and bending, resulting in a value of 0.89 for A/L for case ($D_y = 22.70\delta$ and $D_x = 2$) as shown in Fig. 12(b). The flag flutters as it is affected by external shear layers, leading to the formation of significant vortical structures, which in turn generate a broader wake area which leads to more energy generation.

The normalized frequency values, ranging from 0.035 to 0.088, are illustrated in Fig. 12(c). The maximum values are obtained for $D_y = 34.05\delta$ and $1 \leq D_x \leq 3$ at constant velocity. The value of higher frequency with low amplitude at the specific points can be attributed to the interaction between the piezoelectric flag and the small-scale eddies present in the jet flow. This interaction results in the generation of disturbances, which are caused by the coupling between the flag and the jet flow. The presence of these disturbances leads to interference with the inner shear layers, ultimately resulting in a similar phenomenon. The underlying flow patterns in this system are characterized by an asymmetric and unstable wake for range $11.35\delta \leq D_y \leq 34.05\delta$, which exhibits a bi-stable behaviour due to the continuous deflection of the flexible flag in one direction causes generation of more energy on moving close to the wall but up to certain limit. This measured flip-flop flow instability is attributed to the intrinsic flow characteristics, which are highly sensitive to the system parameters.

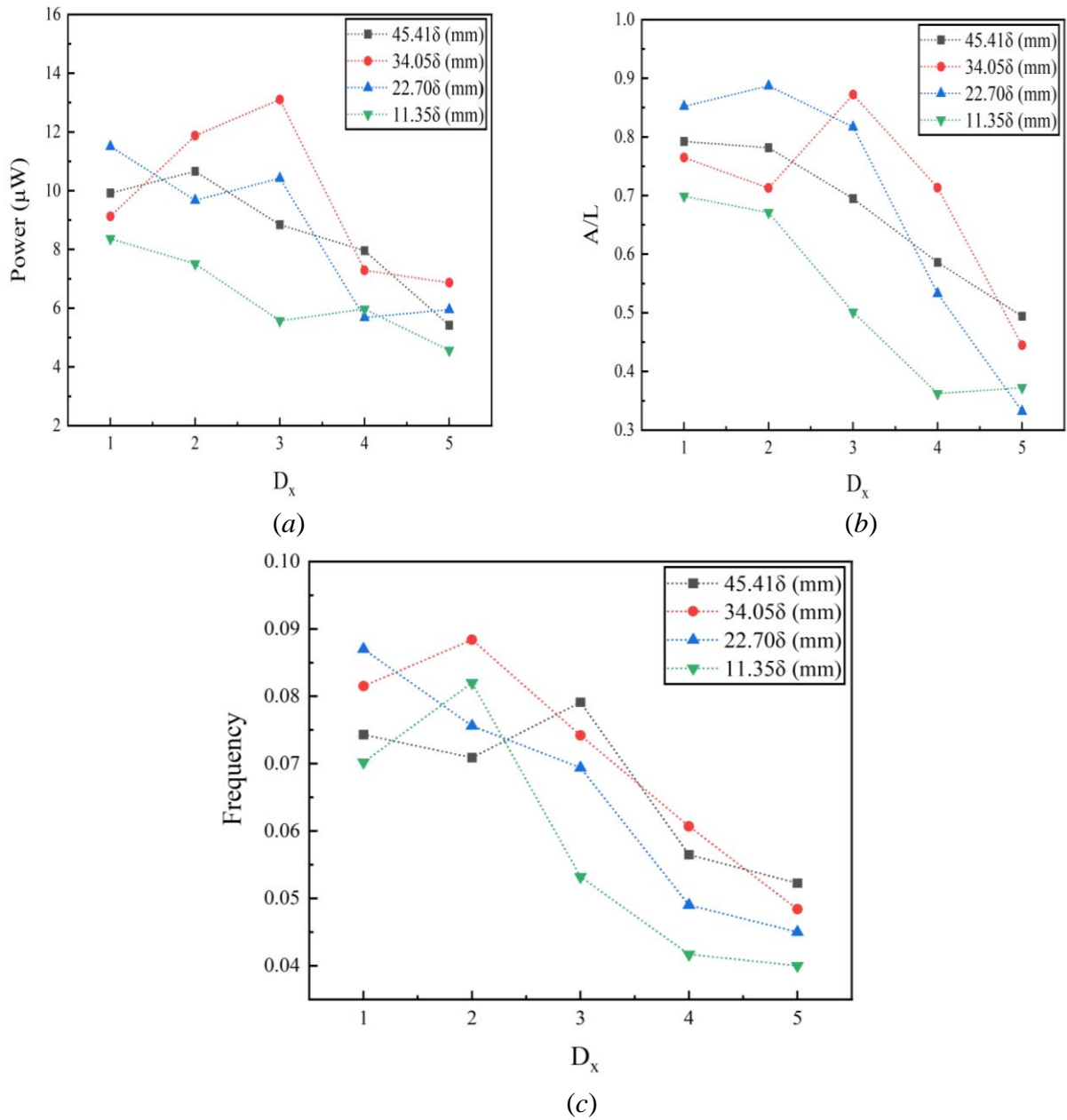


Fig. 12: (a) Power out (b) non-dimensional flapping amplitude (c) dominant frequency for circular cylinder for streamwise gaps ($D_x = 1-5$) and spanwise gaps ($11.35 \leq D_y / \delta \leq 45.41$) for $x^* = 310$ mm at constant velocity.

4.1.4 Experimental Measurements using circular cylinder as bluff body at distance of 310 mm between plates

Next, the configuration featuring an inverted C-shaped cylinder (120° cut) is thoroughly examined. The effects of the gap distance between the bluff body and the energy harvester, as well as the spanwise gap ($11.35\delta \leq D_y \leq 45.41\delta$), are determined through experimental investigations, as presented in Fig. 13. The experimental setup is similar to the previous designs, and the results demonstrate the primary region, characterized by continuous energy

harvesting, is witnessed when the gap distance is in the range of 2 to 3 and D_y is in range $34.05\delta \leq D_y \leq 45.41\delta$. Notably, the energy harvesting behaviour at point $D_y = 34.05\delta$ and $D_x = 3$ depicted in Fig. 13(a) exhibits unique features with highest energy generation.

When the gap distance between the cylindrical bluff body and the cantilever flag is within the range of 2 to 3, the noted dominant frequency and non-dimensional amplitude exhibit a strong dependence on the gap between cylinder and wall of the boundary (D_y). At gap range of $34.05\delta \leq D_y \leq 45.41\delta$ the resultant higher frequency and amplitude contribute to the more energy harvesting as shown by Fig. 13(a) & (b). The outcome of the present configuration reveals that the power output of the circular bluff body ($13.74 \mu\text{W}$) is relatively lower than that of the 120° cut cylinder configuration ($15.67 \mu\text{W}$), exhibiting a higher flapping amplitude of 0.91.

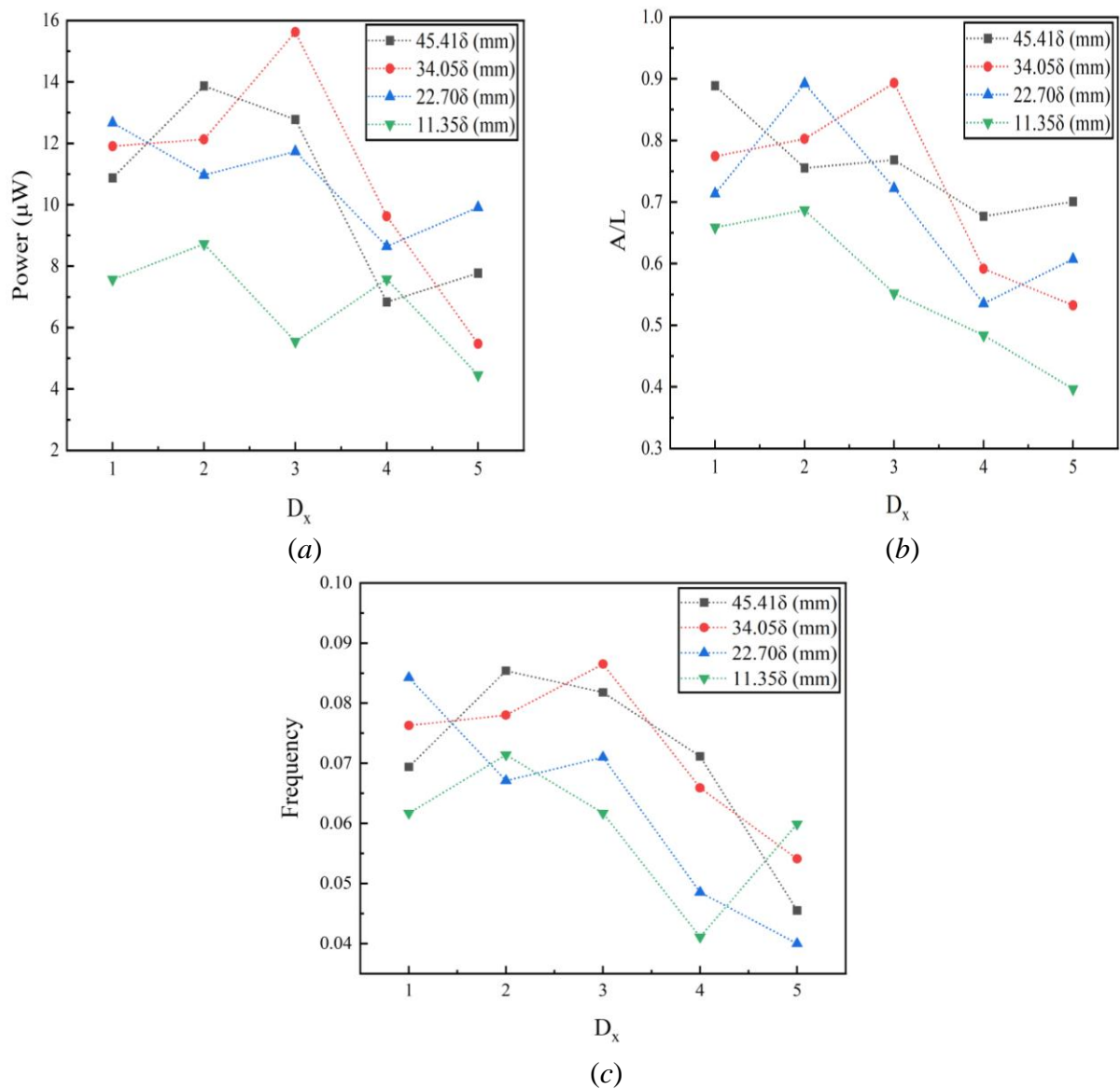
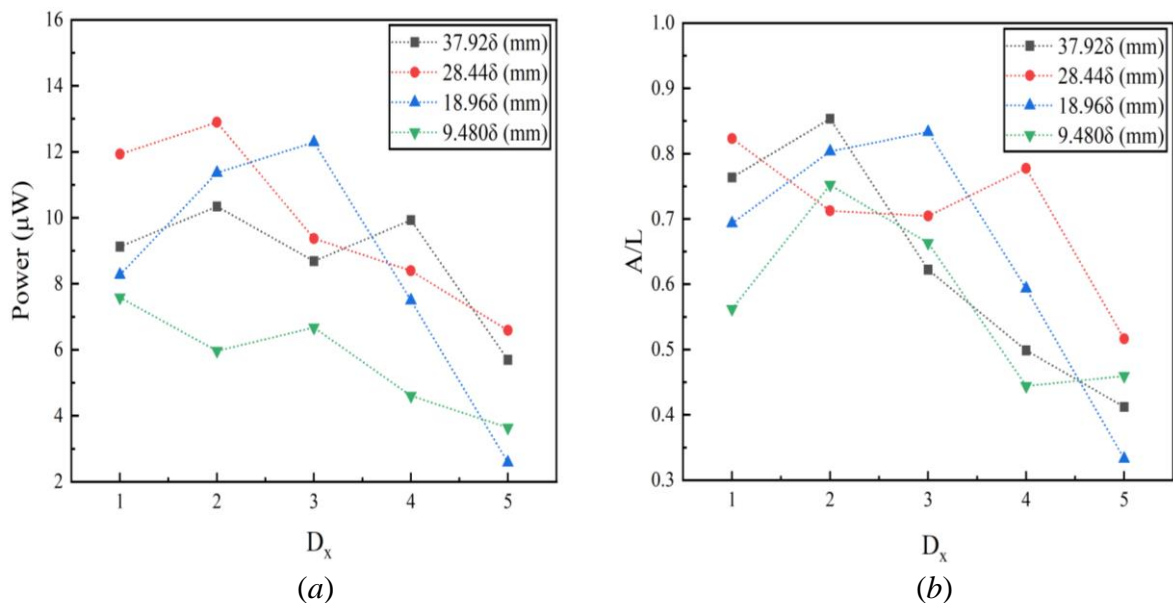


Fig. 13: (a) Power out (b) non-dimensional flapping amplitude (c) dominant frequency for 120° cut inverted C-type cylinder for streamwise gaps ($D_x = 1-5$) and spanwise gaps ($11.35 \leq D_y / \delta \leq 45.41$) for $x^* = 310$ mm at constant velocity.

4.1.5 Experimental Measurements using circular cylinder as bluff body at distance of 260 mm between plates

Upon positioning the piezo flag in the wake of a circular cylinder with $x^* = 260 \text{ mm}$, the experimental findings reveal the emergence of two distinct regions that correspond to high and low levels of harvested power. As shown in Fig. 14(a), the first region ($1 \leq D_x \leq 3$) is associated with high amplitude flapping and high frequency oscillations of the piezo-flag energy harvester for specific value of spanwise distance ($18.96\delta \leq D_y \leq 28.44\delta$). The point $D_y = 28.44\delta$ and $D_x = 2$ in Fig. 14 (a) shows the peak energy harvested. For second region, the low values of power output are experienced due to low amplitude and normalized frequency because of low vortex strength. the minimum power harvested is shown by coordinates $D_y = 18.96\delta$ and $D_x = 5$ in Fig. 14(a). As Kim et al. [94] reported that a flag undergoing flapping motion has the ability to generate a significantly greater amount of elastic strain energy when compared to a flag undergoing deformed motion. This phenomenon can be attributed to the unsteady fluid forces acting on the flag, which result in a more efficient conversion of fluid kinetic energy to elastic strain energy.

Moreover, for $D_y < 28.44\delta$, the harvested power value increases up to certain streamwise gap and then decrease due to establishment of boundary layer and overall, less power is obtained due to more dissipation to overcome viscosity effects. The restricted motion of piezo-flag due to walls effect also leads to low energy generation.



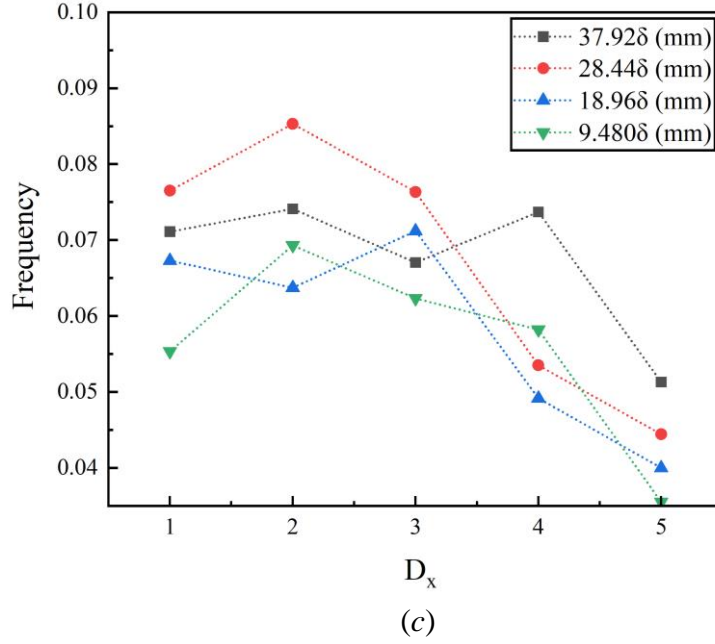


Fig. 14: (a) Power out (b) non-dimensional flapping amplitude (c) dominant frequency for circular cylinder for streamwise gaps ($D_x = 1-5$) and spanwise gaps ($9.48 \leq D_y / \delta \leq 37.92$) for $x^* = 260$ mm at constant velocity.

4.1.6 Experimental Measurements using 120° cut inverted C-type cylinder as bluff body at distance of 260 mm between plates

The outcomes for power output, peak amplitude, and dominant frequency of a C-type inverted cylinder with a 120-degree cut can be seen in Figure 15(a-c) for $x^* = 260$ mm. Upon examining the graph presented in Fig. 15(a), it is evident that the region of greatest energy corresponds to a point where D_x is equal to 3 and D_y is equal to 28.44 δ . Moreover, Fig. 1(b) and 15(c) significantly shows that the maximum flapping amplitude and dominant normalized frequency, respectively, occur at the same streamwise gap ($D_x = 3$). This is due to strong coupling between wake of bluff body and flexible flag. Nevertheless, as depicted in Fig. 7, when the streamwise gap (D_x) between the 120-degree C-shaped cylinder and the cantilevered flag exceeds $D_x = 3$ and the spanwise distance between the cylinder and wall boundary is altered from 18.96 δ to 9.480 δ , there is a reduction in non-dimensional peak amplitude, power output, and normalized frequency as shown in Fig. 15(a-c). These observations suggest the presence of a critical point beyond the prescribed values.

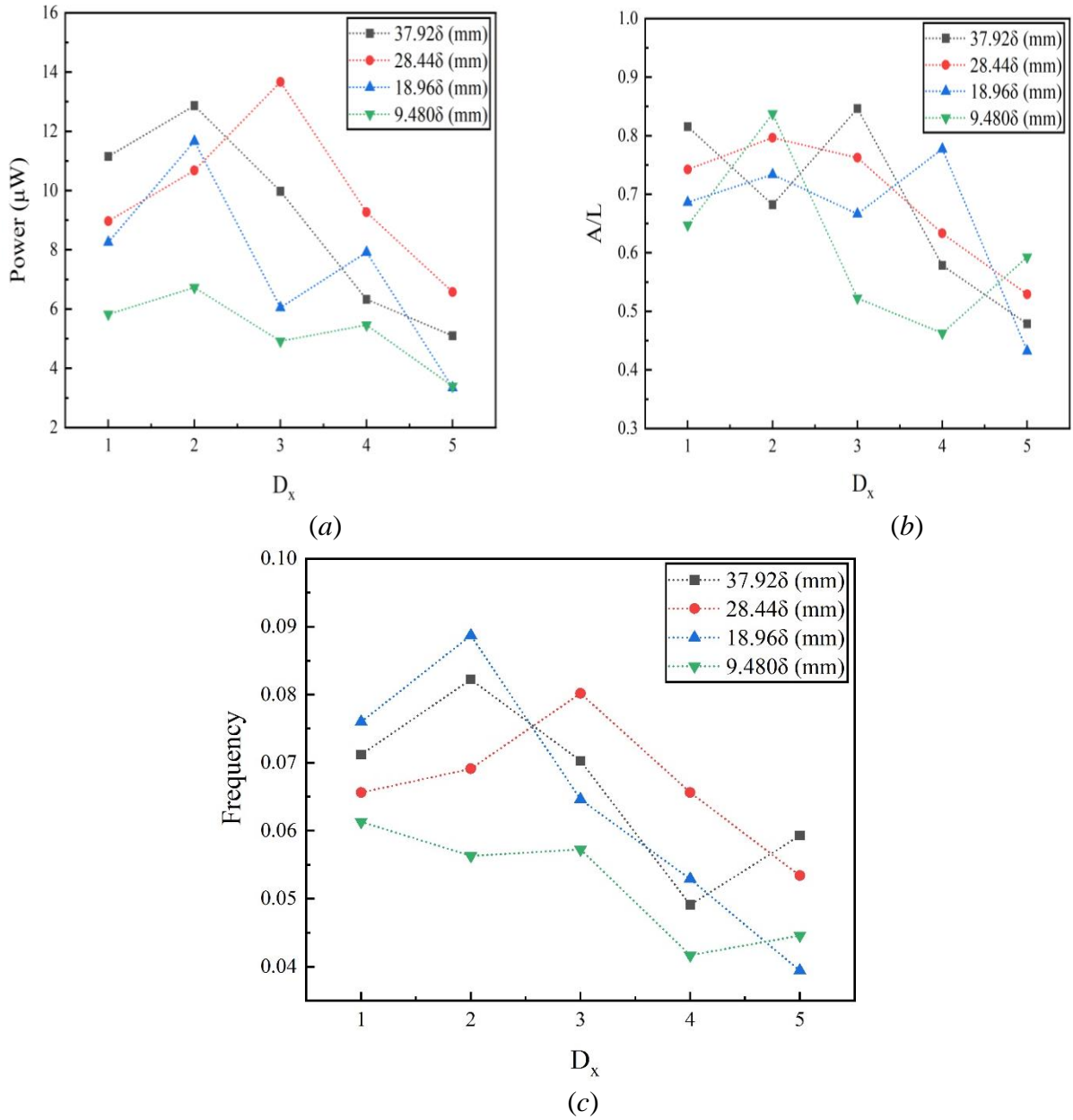


Figure 15: (a) Power out (b) non-dimensional flapping amplitude (c) dominant frequency for 120° cut inverted C-type cylinder for streamwise gaps ($D_x = 1-5$) and spanwise gaps ($9.48 \leq D_y / \delta \leq 37.92$) for $x^* = 260$ mm at constant velocity.

4.2 Comparative Analysis and Optimal Configuration

Fig. 16 illustrates the comparison of the highest amount of power generated by using a piezoelectric flag positioned behind circular and 120 degree cut inverted C-type cylindrical bluff bodies for different values of D_x , D_y and x^* to study the impact of boundary layer thickness. It is clear in Fig. 16(a) that the highest power output of 13.10 μW is achieved when

a flag is positioned at a distance of $D_x = 3.0$ in the wake of the circular bluff body for $x^* = 310$ mm and $D_y = 34.05\delta$. The use of a piezoelectric eel positioned behind 120° cut C-type cylindrical bluff bodies yields a maximum power output of $15.62 \mu\text{W}$, as shown in Fig. 16(b). This amount is 83% higher than the power generated for simple cylindrical body validating the results in literature also. The setting of cylindrical bluff bodies with $x^* = 310$ mm shows continuous oscillation of flexible flag results in more power generation for wide range of $D_x = 2-3$ and $D_y = 22.70\delta-34.05\delta$. The instantaneous values of voltages for maximum and minimum configurations among all are shown in Fig. 17(a) & (b) respectively.

The experimental results presented in Fig. 16 indicate the significant advantages of deploying cylinder configuration in various high-tech applications, including aerospace technology, wind turbines, offshore pipelines, and hydroelectric power plants. The substantial power output generated by this approach can effectively power several data acquisition systems, data processing units, and communication devices that are critical for the efficient operation of these systems. Furthermore, the high-performance capabilities of these systems facilitate real-time data acquisition, analysis, and storage, thereby enabling users to make informed decisions and optimize system performance by launching self-sustainable systems. Though continuous power can be harvested using different bluff bodies and gaps for different distances between plates, optimal position is necessary to make the closed device self-sustainable. The reason is that for spanwise gaps close to the walls the fluid viscous impacts are significant and flapping of eel is restricted. In the current study, the optimal position for both the bluff bodies is for ranges $2 \leq D_x \leq 3$ and $22.70 \leq D_y/\delta \leq 34.05$ when the distance between plates is 310 mm because of high value of dominant frequency and non-dimensional amplitude (A/L). This shows, a higher amplitude results in increased power output, while frequency is directly linked to strain rate. This means that high strain rates produce more energy in less time, which is advantageous for fast charging cycle of battery. Both parameters have a direct impact on power generation, and a device with higher amplitude is more feasible as it produces more strain at a given frequency. In other cases where high amplitude and low frequency are present, peak to peak output voltages are high. Conversely, low amplitude with high frequency results in low peak to peak output voltage. Hence, a superior device is one that can generate energy with both parameters high.

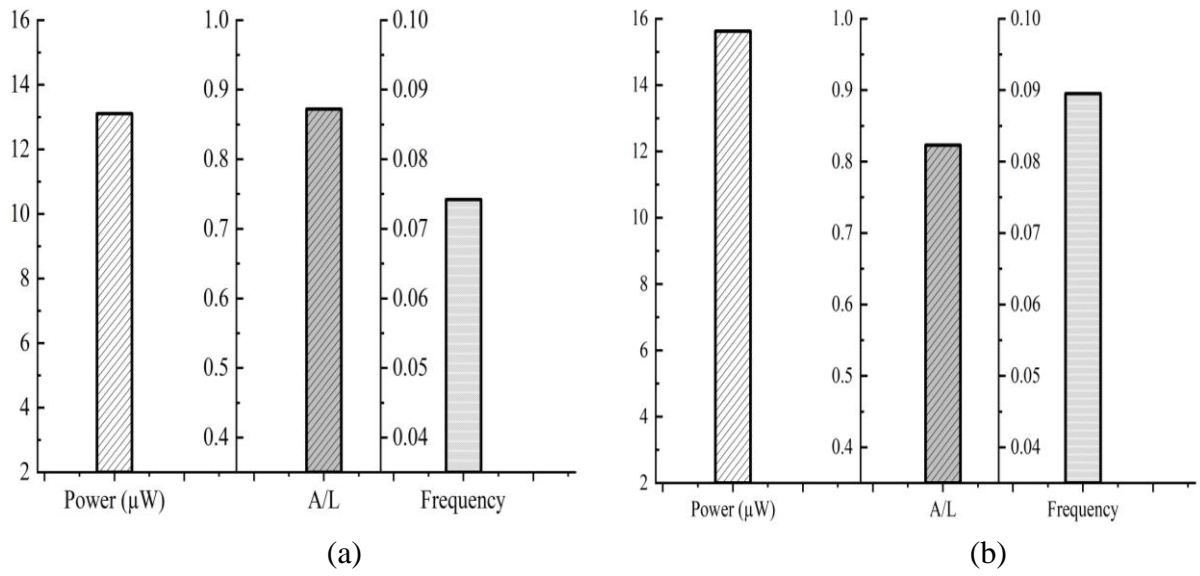


Fig. 16: (a) Power, A/L ratio and Flapping Frequency for maximum configuration among all for circular cylinder at point $D_x = 3$, $D_y = 34.05\delta$ for $x^* = 310$ mm (b) Power, A/L ratio and Flapping Frequency for maximum configuration among all for 120° degree cut C-type

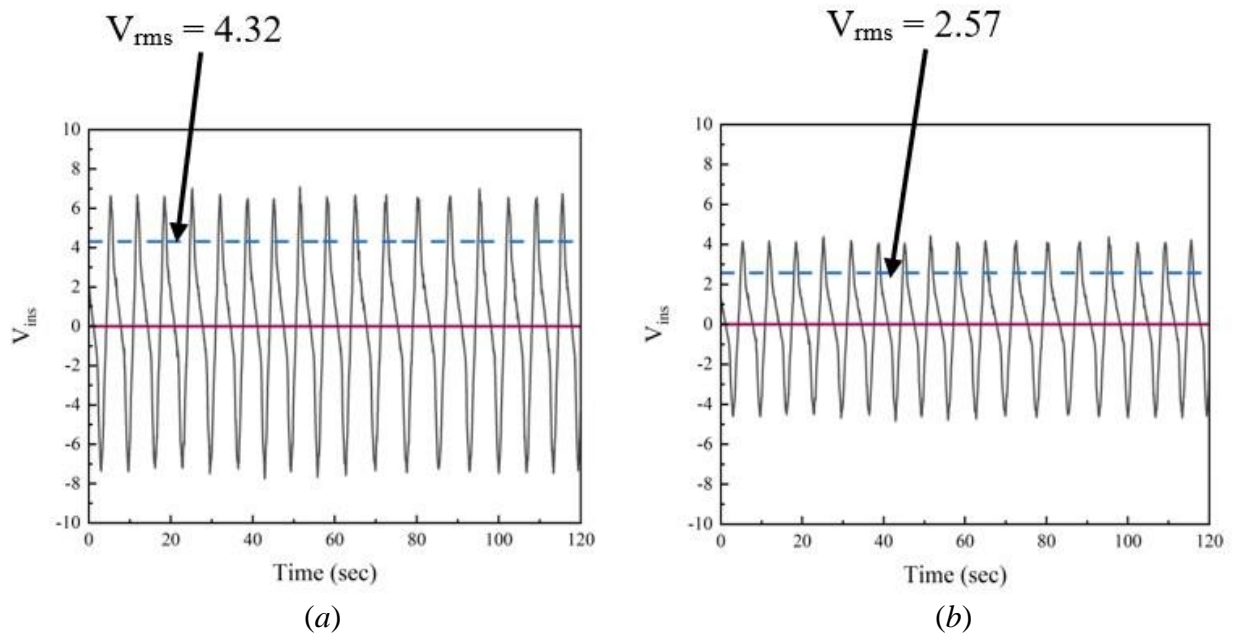


Fig. 17: (a) RMS and Instantaneous Voltage for maximum output configuration for 120° cut C-type inverted cylinder at point $D_x = 3$, $D_y = 34.05\delta$ for $x^* = 310$ mm (b) RMS and Instantaneous Voltage for minimum output configuration for circular cylinder at point $D_x = 5$, $D_y = 18.96\delta$ for $x^* = 260$ mm

Particle image velocimetry (PIV) flow is used to analyse the wake (time-averaged) of cylinders in order to better understand wake features and discover the relationship between varying cross-sections and altered energy harvesting behaviour. The mean streamlines of vorticity for all bluff bodies are shown in Fig. 18. Using one, the results are time-averaged using one thousand instantaneous PIV observations in '.dat' files. For both circular and 120 degree cut cylinders, the PIV view window extends $5d$ in a stream-wise direction. The view spans $3d$ in the transverse direction. The flow splitting off from the cylinder surface, which also initiates the free shear layer instability, results in the production of a vortical flow structure and the subsequent expansion of the wake region/flow as shown in Fig. 18. The vortex may have moved momentum, mass, and flow energy across a significant downstream distance before dissipating. As a result, the movement of mass and angular momentum causes the fluid to transfer kinetic energy to a flexible structure (the piezo-membrane), which in turn causes time-dependent strain through the interaction of alternating shedded vortices with opposite signs.

Fig. 18(a-d) shows that the highest energy output for a circular cylinder occurs when the piezoelectric flag is set at $D_x = 3$, coinciding with the location of the vortex core. Likewise, when the flag head is fixed at D_x for a 120-degree cut angle, the vortex core aligns with the same location of maximum energy output from the piezoelectric flag positioned behind the cylinder. The literature clearly indicates that the vortex core exhibits the highest strength due to its maximum circulation [95]. Therefore, to extract the maximum energy from the vortex, it is crucial to position the piezoelectric flag near the location where the vortex core converges. In this arrangement, the traveling vortex will efficiently transfer its kinetic energy to the flag, resulting in the conversion of mechanical energy into strain energy.

A further analysis and comparison of Fig. 18(a) & (c) shed light on the reasons behind the enhanced energy generation observed when the flag was positioned behind a 120-degree cut cylinder. Fig. 18(c) clearly shows that the presumed vortices possess greater strength and size in all aspects. As a result, there is a higher flow/mechanical energy transfer to the piezoelectric flag, leading to increased electrical energy generation. Fig. 18(c) & (d) shows minimum energy generation due to significant viscous effects in the proximity of wall boundary. It is evident that higher forces result in greater strain, manifested as deformation of the piezoelectric flag, which directly impacts energy generation. Consequently, stronger vortices lead to a higher level of impingement, resulting in greater harvested energy.

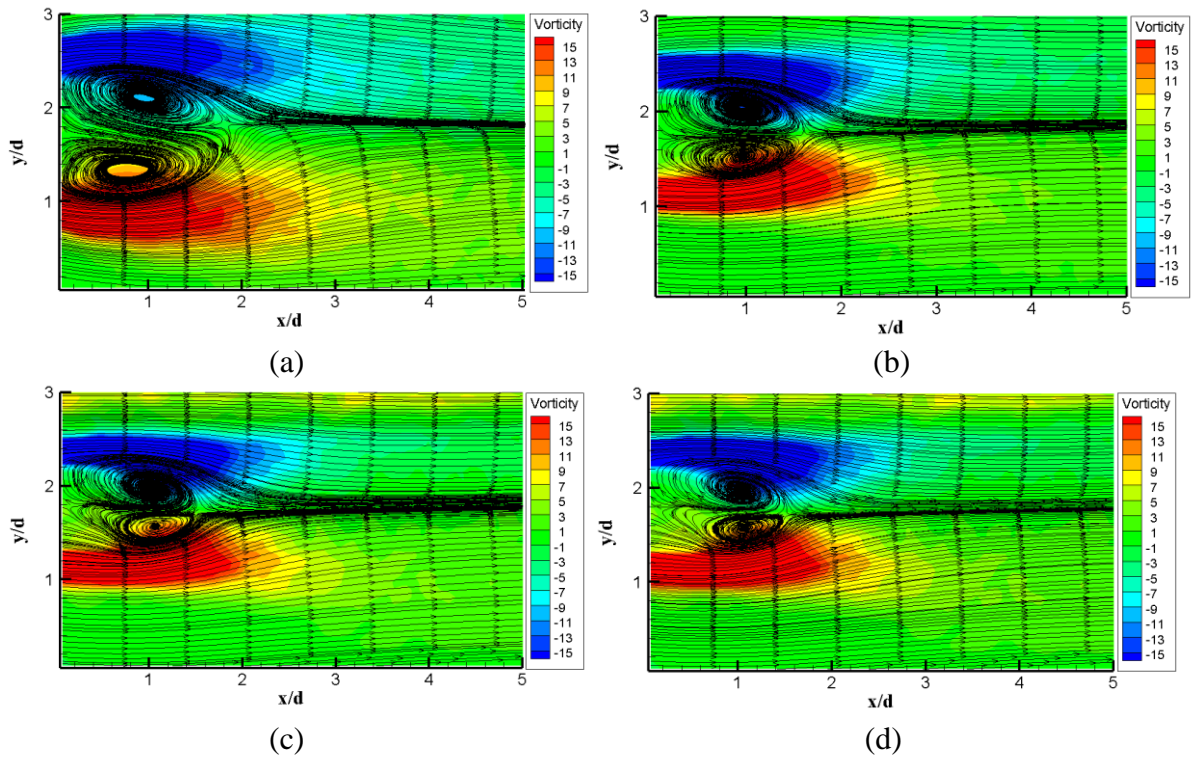


Fig. 18: PIV Result for maximum and minimum energy generation cases taken by taking the average of 1000 images

Chapter 5

Conclusion

The impact of boundary layer thickness by varying the distance between side plate boundaries ($260 \leq x^* \leq 360$) mm on the performance of energy harvester was investigated and discussed in this experimental study. Circular and 120 degree cut C-type inverted cylinder were used as bluff bodies to disturb the flow and create strong wake. The streamwise and spanwise gaps between cylinder to cantilevered flag and cylinder to plate boundary were subjected to variation for each channel width to determine the optimal arrangement of the harvester. The flapping frequency and amplitude response were compared at each point for all configurations to understand the impact of variable parameters on the results and trends. For $x^* = 310$ mm, the cylinder arrangement with $G_x = 2.0-3.0$ sustained higher output power for wider range $22.70 \leq G_y / \delta \leq 34.05$, which makes it suitable choice for practical applications involving low flow velocities. Though a circular bluff body can be used to generate continuous power, but 120 degree cut C-type cylinder resulted in 83% more power generation for the same cylindrical arrangement because of larger wake width and strong coupling with energy harvester. The arrangement with $x^* = 310$ mm yielded a wake width that was greater in magnitude, resulting in an approximately 168% increase in non-dimensional amplitude (A/L) as compared to other configurations. Further, sudden drop in power output was found for $9.480 \leq G_y / \delta \leq 18.96$ with 260 mm distance between side boundaries due to boundary layer viscous effects, restricted flapping of piezo-flag and poor coupling of wake flow. The energy harvesting potential of piezoelectric harvester for these configurations varies from 2.58 μ W to 15.62 μ W, illustrating an impressive 505% surge in power generation by selecting the optimal configuration for energy harvesting. The energy generated is completely renewable and environmentally friendly, making it a sustainable and practical solution for powering microelectronic devices such as sensors used in remote areas and Internet of Things (IoT) applications. In addition to its benefits for the environment, this technology can also reduce reliance on traditional power sources and eliminate the need for small, disposable batteries.

To comprehensively investigate the energy harvesting capabilities, it would be beneficial to expand the study to include other techniques such as galloping. Additionally, practical implementation of the proposed energy harvester in real-world scenarios is necessary to broaden its scope and evaluate its efficiency. Furthermore, for future endeavors, it would be beneficial to conduct thorough numerical simulations with closed channels incorporating top and bottom plates also for making self-sustaining portable devices.

References

- [1] Sudevalayam, S., and Kulkarni, P., 2011, "Energy Harvesting Sensor Nodes: Survey and Implications," *IEEE Commun. Surv. Tutorials*, **13**(3), pp. 443–461.
- [2] Priya, S., 2007, "Advances in Energy Harvesting Using Low Profile Piezoelectric Transducers," *J. Electroceramics*, **19**(1), pp. 165–182.
- [3] Basagni, S., Naderi, M. Y., Petrioli, C., and Spenza, D., 2013, "Wireless Sensor Networks with Energy Harvesting," *Mob. Ad Hoc Netw. Cut. Edge Dir. Second Ed.*, pp. 701–736.
- [4] Yu, H., and Yue, Q., 2012, "Indoor Light Energy Harvesting System for Energy-Aware Wireless Sensor Node," *Energy Procedia*, **16**(PART B), pp. 1027–1032.
- [5] Glynne-Jones, P., Tudor, M. J., Beeby, S. P., and White, N. M., 2004, "An Electromagnetic, Vibration-Powered Generator for Intelligent Sensor Systems," *Sensors Actuators, A Phys.*, **110**(1–3), pp. 344–349.
- [6] Vullers, R. J. M., van Schaijk, R., Doms, I., Van Hoof, C., and Mertens, R., 2009, "Micropower Energy Harvesting," *Solid. State. Electron.*, **53**(7), pp. 684–693.
- [7] Harb, A., 2011, "Energy Harvesting: State-of-the-Art," *Renew. Energy*, **36**(10), pp. 2641–2654.
- [8] Coe, S. I. T., 2016, "PIEZOELECTRIC MOTORS & IT ' S APPLICATIONS Miss : Neelima Sharad Vatkar," *Int. Res. J. Eng. Technol.*, **3**(6), pp. 986–990.
- [9] Ramadan, K. S., Sameoto, D., and Evoy, S., 2014, "A Review of Piezoelectric Polymers as Functional Materials for Electromechanical Transducers," *Smart Mater. Struct.*, **23**(3).
- [10] Tang, L., Païdoussis, M. P., and Jiang, J., 2009, "Cantilevered Flexible Plates in Axial Flow: Energy Transfer and the Concept of Flutter-Mill," *J. Sound Vib.*, **326**(1–2), pp. 263–276.
- [11] Techet, A. H., Allen, J. J., and Smits, A. J., 2002, "Piezoelectric Eels for Energy Harvesting in the Ocean," *Proc. Int. Offshore Polar Eng. Conf.*, **12**, pp. 713–718.
- [12] Singh, K., Michelin, S., and de Langre, E., 2012, "Energy Harvesting from Axial Fluid-Elastic Instabilities of a Cylinder," *J. Fluids Struct.*, **30**, pp. 159–172.
- [13] Dunnmon, J. A., Stanton, S. C., Mann, B. P., and Dowell, E. H., 2011, "Power Extraction from Aeroelastic Limit Cycle Oscillations," *J. Fluids Struct.*, **27**(8), pp. 1182–1198.
- [14] Erturk, A., Vieira, W. G. R., De Marqui, C., and Inman, D. J., 2010, "On the Energy Harvesting Potential of Piezoaeroelastic Systems," *Appl. Phys. Lett.*, **96**(18).
- [15] Barrero-Gil, A., Alonso, G., and Sanz-Andres, A., 2010, "Energy Harvesting from Transverse Galloping," *J. Sound Vib.*, **329**(14), pp. 2873–2883.
- [16] Matiko, J. W., Grabham, N. J., Beeby, S. P., and Tudor, M. J., 2014, "Review of the Application of Energy Harvesting in Buildings," *Meas. Sci. Technol.*, **25**(1).
- [17] Zahid Kausar, A. S. M., Reza, A. W., Saleh, M. U., and Ramiah, H., 2014, "Energizing Wireless Sensor Networks by Energy Harvesting Systems: Scopes, Challenges and

- Approaches,” *Renew. Sustain. Energy Rev.*, **38**, pp. 973–989.
- [18] Panwar, N. L., Kaushik, S. C., and Kothari, S., 2011, “Role of Renewable Energy Sources in Environmental Protection: A Review,” *Renew. Sustain. Energy Rev.*, **15**(3), pp. 1513–1524.
- [19] Karim, M. E., Munir, A. B., Karim, M. A., Muhammad-Sukki, F., Abu-Bakar, S. H., Sellami, N., Bani, N. A., and Hassan, M. Z., 2018, “Energy Revolution for Our Common Future: An Evaluation of the Emerging International Renewable Energy Law,” *Energies*, **11**(7).
- [20] Umair, M., Latif, U., Uddin, E., and Abdelkefi, A., 2022, “Experimental Hydrodynamic Investigations on the Effectiveness of Inverted Flag-Based Piezoelectric Energy Harvester in the Wake of Bluff Body,” *Ocean Eng.*, **245**(August 2021), p. 110454.
- [21] Ball, A. D., Gu, F., Cattley, R., Wang, X., and Tang, X., 2018, “Energy Harvesting Technologies for Achieving Self-Powered Wireless Sensor Networks in Machine Condition Monitoring: A Review,” *Sensors (Switzerland)*, **18**(12).
- [22] Song, G. J., Cho, J. Y., Kim, K. B., Ahn, J. H., Song, Y., Hwang, W., Hong, S. Do, and Sung, T. H., 2019, “Development of a Pavement Block Piezoelectric Energy Harvester for Self-Powered Walkway Applications,” *Appl. Energy*, **256**(April), p. 113916.
- [23] Wang, C., Zhao, J., Li, Q., and Li, Y., 2018, “Optimization Design and Experimental Investigation of Piezoelectric Energy Harvesting Devices for Pavement,” *Appl. Energy*, **229**(June), pp. 18–30.
- [24] Mujtaba, A., Latif, U., Uddin, E., Younis, M. Y., Sajid, M., Ali, Z., and Abdelkefi, A., 2021, “Hydrodynamic Energy Harvesting Analysis of Two Piezoelectric Tandem Flags under Influence of Upstream Body’s Wakes,” *Appl. Energy*, **282**(August 2020).
- [25] Sultana, A., Alam, M. M., Middy, T. R., and Mandal, D., 2018, “A Pyroelectric Generator as a Self-Powered Temperature Sensor for Sustainable Thermal Energy Harvesting from Waste Heat and Human Body Heat,” *Appl. Energy*, **221**(January), pp. 299–307.
- [26] Lü, C., Zhang, Y., Zhang, H., Zhang, Z., Shen, M., and Chen, Y., 2019, “Generalized Optimization Method for Energy Conversion and Storage Efficiency of Nanoscale Flexible Piezoelectric Energy Harvesters,” *Energy Convers. Manag.*, **182**(December 2018), pp. 34–40.
- [27] Izadgoshasb, I., Lim, Y. Y., Lake, N., Tang, L., Padilla, R. V., and Kashiwao, T., 2018, “Optimizing Orientation of Piezoelectric Cantilever Beam for Harvesting Energy from Human Walking,” *Energy Convers. Manag.*, **161**(January), pp. 66–73.
- [28] Bhaskaran, J., 2022, “Journal of Nuclear Energy Science & Power Generation Technology Sustainable Energy Harvesting for Self-Powered Micro / Nanosystems Enabled by Nanotechnology,” (March).
- [29] Wang, Z. L., 2012, “Self-Powered Nanosensors and Nanosystems,” *Adv. Mater.*, **24**(2), pp. 280–285.
- [30] Wu, Z., Cheng, T., and Wang, Z. L., 2020, “Self-Powered Sensors and Systems Based on Nanogenerators,” *Sensors (Switzerland)*, **20**(10).
- [31] Watson, S., Moro, A., Reis, V., Baniotopoulos, C., Barth, S., Bartoli, G., Bauer, F., Boelman, E., Bosse, D., Cherubini, A., Croce, A., Fagiano, L., Fontana, M., Gambier, A., Gkoumas, K., Golightly, C., Latour, M. I., Jamieson, P., Kaldellis, J., Macdonald,

- A., Murphy, J., Muskulus, M., Petrini, F., Pigolotti, L., Rasmussen, F., Schild, P., Schmehl, R., Stavridou, N., Tande, J., Taylor, N., Telsnig, T., and Wiser, R., 2019, “Future Emerging Technologies in the Wind Power Sector: A European Perspective,” *Renew. Sustain. Energy Rev.*, **113**(November 2018), p. 109270.
- [32] Elahi, H., Eugeni, M., Fune, F., Lampani, L., Mastroddi, F., Romano, G. P., and Gaudenzi, P., 2020, “Performance Evaluation of a Piezoelectric Energy Harvester Based on Flag-Flutter,” *Micromachines*, **11**(10).
- [33] Latif, U., Abdullah, C., Uddin, E., Younis, M. Y., Sajid, M., Shah, S. R., and Mubasha, A., 2018, “Experimental and Numerical Investigation of the Energy Harvesting Flexible Flag in the Wake of a Bluff Body,” *Wind Struct. An Int. J.*, **26**(5), pp. 279–292.
- [34] Usman, M., Hanif, A., Kim, I. H., and Jung, H. J., 2018, “Experimental Validation of a Novel Piezoelectric Energy Harvesting System Employing Wake Galloping Phenomenon for a Broad Wind Spectrum,” *Energy*, **153**, pp. 882–889.
- [35] Latif, U., Younis, M. Y., Idrees, S., Uddin, E., Abdelkefi, A., Munir, A., and Zhao, M., 2023, “Synergistic Analysis of Wake Effect of Two Cylinders on Energy Harvesting Characteristics of Piezoelectric Flag,” *Renew. Sustain. Energy Rev.*, **173**(July 2022), p. 113114.
- [36] Williamson, C. H. K., 1996, “Vortex Dynamics in the Cylinder Wake,” *Annu. Rev. Fluid Mech.*, **28**, pp. 477–539.
- [37] Akaydin, H. D., Elvin, N., and Andreopoulos, Y., 2012, “The Performance of a Self-Excited Fluidic Energy Harvester,” *Smart Mater. Struct.*, **21**(2).
- [38] Gowdhaman, P., Antonyraj, K., and Annamalai, V., 2015, “An Effective Approach on Physical and Dielectric Properties of PZT- PVDF Composites,” *Int. J. Adv. Sci. Res.*, **1**(08), pp. 322–328.
- [39] Levin, D., and Dowell, E. H., 2019, “Improving Piezoelectric Energy Harvesting from an Aeroelastic System,” *Int. Forum Aeroelasticity Struct. Dyn. 2019, IFASD 2019*, (June), pp. 1–37.
- [40] Jain, A., Prashanth, K. J., Sharma, A. K., Jain, A., and P.n, R., 2015, “Dielectric and Piezoelectric Properties of PVDF/PZT Composites: A Review,” *Polym. Eng. Sci.*, **55**(7), pp. 1589–1616.
- [41] Sooraj, P., Khan, M. H., Sharma, A., and Agrawal, A., 2019, “Wake Analysis and Regimes for Flow around Three Side-by-Side Cylinders,” *Exp. Therm. Fluid Sci.*, **104**(December 2018), pp. 76–88.
- [42] Wang, E., Xu, W., Yu, Y., Zhou, L., and Incecik, A., 2019, “Flow-Induced Vibrations of Three and Four Long Flexible Cylinders in Tandem Arrangement: An Experimental Study,” *Ocean Eng.*, **178**(January), pp. 170–184.
- [43] U, L., and Shah A, N., 2016, “Design and Analysis of a Tension Leg Platforms Column for Arabian Sea,” *J. Appl. Mech. Eng.*, **5**(4).
- [44] Yu, Y., Liu, Y., and Chen, Y., 2017, “Vortex Dynamics behind a Self-Oscillating Inverted Flag Placed in a Channel Flow: Time-Resolved Particle Image Velocimetry Measurements,” *Phys. Fluids*, **29**(12), pp. 0–15.
- [45] Wang, J., Geng, L., Ding, L., Zhu, H., and Yurchenko, D., 2020, “The State-of-the-Art Review on Energy Harvesting from Flow-Induced Vibrations,” *Appl. Energy*, **267**(March), p. 114902.

- [46] Virot, E., Amandolese, X., and Hémon, P., 2013, “Fluttering Flags: An Experimental Study of Fluid Forces,” *J. Fluids Struct.*, **43**, pp. 385–401.
- [47] Alben, S., 2015, “Flag Flutter in Inviscid Channel Flow,” *Phys. Fluids*, **27**(3), pp. 1–25.
- [48] Perez, M., Boisseau, S., Gasnier, P., Willemin, J., and Reboud, J. L., 2015, “An Electret-Based Aeroelastic Flutter Energy Harvester,” *Smart Mater. Struct.*, **24**(3).
- [49] Beal, D. N., Hover, F. S., Triantafyllou, M. S., Liao, J. C., and Lauder, G. V., 2006, “Passive Propulsion in Vortex Wakes,” *J. Fluid Mech.*, **549**, pp. 385–402.
- [50] Taylor, G. W., Burns, J. R., Kammann, S. M., Powers, W. B., and Welsh, T. R., 2001, “The Energy Harvesting Eel: A Small Subsurface Ocean/River Power Generator,” *IEEE J. Ocean. Eng.*, **26**(4), pp. 539–547.
- [51] Shi, S., New, T. H., and Liu, Y., 2013, “Flapping Dynamics of a Low Aspect-Ratio Energy-Harvesting Membrane Immersed in a Square Cylinder Wake,” *Exp. Therm. Fluid Sci.*, **46**(November 2017), pp. 151–161.
- [52] Pan, F., Xu, Z., Jin, L., Pan, P., and Gao, X., 2017, “Designed Simulation and Experiment of a Piezoelectric Energy Harvesting System Based on Vortex-Induced Vibration,” *IEEE Trans. Ind. Appl.*, **53**(4), pp. 3890–3897.
- [53] Tanaka, Y., Oko, T., Mutsuda, H., Patel, R., McWilliam, S., and Popov, A. A., 2015, “An Experimental Study of Wave Power Generation Using a Flexible Piezoelectric Device,” *J. Ocean Wind Energy*, **2**(1), pp. 28–36.
- [54] Gkoumas, K., Petrini, F., and Bontempi, F., 2012, “Energy Harvesting for the Life-Cycle of Structures and Infrastructures: State of Art, Recent Trends and Future Developments,” *Life-Cycle Sustain. Civ. Infrastruct. Syst. - Proc. 3rd Int. Symp. Life-Cycle Civ. Eng. IALCCE 2012*, (June 2014), pp. 2102–2109.
- [55] Wang, D. A., Chiu, C. Y., and Pham, H. T., 2012, “Electromagnetic Energy Harvesting from Vibrations Induced by Kármán Vortex Street,” *Mechatronics*, **22**(6), pp. 746–756.
- [56] Hassan, M. M., Hossain, M. Y., Mazumder, R., Rahman, R., and Rahman, M. A., 2016, “Vibration Energy Harvesting in a Small Channel Fluid Flow Using Piezoelectric Transducer,” *AIP Conf. Proc.*, **1754**(July).
- [57] Shi, S., New, T. H., and Liu, Y., 2014, “Effects of Aspect-Ratio on the Flapping Behaviour of Energy-Harvesting Membrane,” *Exp. Therm. Fluid Sci.*, **52**, pp. 339–346.
- [58] Kim, S., Huang, W. X., and Sung, H. J., 2010, “Constructive and Destructive Interaction Modes between Two Tandem Flexible Flags in Viscous Flow,” *J. Fluid Mech.*, **661**, pp. 511–521.
- [59] Hu, G., Liu, F., Li, L., Li, C., Xiao, Y., and Kwok, K. C. S., 2019, “Wind Energy Harvesting Performance of Tandem Circular Cylinders with Triangular Protrusions,” *J. Fluids Struct.*, **91**, p. 102780.
- [60] Zhao, F., Jiang, Q., Wang, Z., Qadri, M. N. M., Li, L., and Tang, H., 2023, “Interaction of Two Fully Passive Flapping Foils Arranged in Tandem and Its Influence on Flow Energy Harvesting,” *Energy*, **268**(January), p. 126714.
- [61] Mujtaba, A., Latif, U., Uddin, E., Younis, M. Y., Sajid, M., Ali, Z., and Abdelkefi, A., 2021, “Hydrodynamic Energy Harvesting Analysis of Two Piezoelectric Tandem Flags under Influence of Upstream Body’s Wakes,” *Appl. Energy*, **282**(August 2020).
- [62] Shan, X., Song, R., Fan, M., and Xie, T., 2016, “Energy-Harvesting Performances of Two Tandem Piezoelectric Energy Harvesters with Cylinders in Water,” *Appl. Sci.*,

- 6(8).
- [63] Hu, G., Tse, K. T., Wei, M., Naseer, R., Abdelkefi, A., and Kwok, K. C. S., 2018, “Experimental Investigation on the Efficiency of Circular Cylinder-Based Wind Energy Harvester with Different Rod-Shaped Attachments,” *Appl. Energy*, **226**(May), pp. 682–689.
- [64] Latif, U., Uddin, E., Younis, M. Y., Aslam, J., Ali, Z., Sajid, M., and Abdelkefi, A., 2021, “Experimental Electro-Hydrodynamic Investigation of Flag-Based Energy Harvesting in the Wake of Inverted C-Shape Cylinder,” *Energy*, **215**.
- [65] Wang, J., Zhou, S., Zhang, Z., and Yurchenko, D., 2019, “High-Performance Piezoelectric Wind Energy Harvester with Y-Shaped Attachments,” *Energy Convers. Manag.*, **181**(December 2018), pp. 645–652.
- [66] Gibbs, S. C., Fichera, S., Zanotti, A., Ricci, S., and Dowell, E. H., 2014, “Flow Field around the Flapping Flag,” *J. Fluids Struct.*, **48**(2003), pp. 507–513.
- [67] Latif, U., and By, S., 2021, “Experimental Study of Energy Harvesting Flag under the Influence of Wakes Experimental Study of Energy Harvesting Flag under the Influence of Wakes.”
- [68] Gu, M., Song, B., Zhang, B., Mao, Z., and Tian, W., 2020, “The Effects of Submergence Depth on Vortex-Induced Vibration (VIV) and Energy Harvesting of a Circular Cylinder,” *Renew. Energy*, **151**, pp. 931–945.
- [69] Abdelkefi, A., Scanlon, J. M., McDowell, E., and Hajj, M. R., 2013, “Performance Enhancement of Piezoelectric Energy Harvesters from Wake Galloping,” *Appl. Phys. Lett.*, **103**(3).
- [70] Zhou, K., Dai, H. L., Abdelkefi, A., and Ni, Q., 2020, “Theoretical Modeling and Nonlinear Analysis of Piezoelectric Energy Harvesters with Different Stoppers,” *Int. J. Mech. Sci.*, **166**(June 2019).
- [71] Zhao, L., Tang, L., and Yang, Y., 2013, “Comparison of Modeling Methods and Parametric Study for a Piezoelectric Wind Energy Harvester,” *Smart Mater. Struct.*, **22**(12).
- [72] Rezaei, M., Talebitooti, R., and Rahmanian, S., 2019, “Efficient Energy Harvesting from Nonlinear Vibrations of PZT Beam under Simultaneous Resonances,” *Energy*, **182**, pp. 369–380.
- [73] Rezaei, M., and Talebitooti, R., 2019, “Wideband PZT Energy Harvesting from the Wake of a Bluff Body in Varying Flow Speeds,” *Int. J. Mech. Sci.*, **163**(June).
- [74] He, X., Yang, X., and Jiang, S., 2018, “Enhancement of Wind Energy Harvesting by Interaction between Vortex-Induced Vibration and Galloping,” *Appl. Phys. Lett.*, **112**(3).
- [75] Kwon, S. D., 2010, “A T-Shaped Piezoelectric Cantilever for Fluid Energy Harvesting,” *Appl. Phys. Lett.*, **97**(16), pp. 1–4.
- [76] Liu, F. R., Zou, H. X., Zhang, W. M., Peng, Z. K., and Meng, G., 2018, “Y-Type Three-Blade Bluff Body for Wind Energy Harvesting,” *Appl. Phys. Lett.*, **112**(23), pp. 1–6.
- [77] Ding, L., Zhang, L., Wu, C., Mao, X., and Jiang, D., 2015, “Flow Induced Motion and Energy Harvesting of Bluff Bodies with Different Cross Sections,” *Energy Convers. Manag.*, **91**, pp. 416–426.
- [78] Zhao, D., Hu, X., Tan, T., Yan, Z., and Zhang, W., 2020, “Piezoelectric Galloping

- Energy Harvesting Enhanced by Topological Equivalent Aerodynamic Design,” *Energy Convers. Manag.*, **222**(August), p. 113260.
- [79] Mehmood, A., Abdelkefi, A., Hajj, M. R., Nayfeh, A. H., Akhtar, I., and Nuhait, A. O., 2013, “Piezoelectric Energy Harvesting from Vortex-Induced Vibrations of Circular Cylinder,” *J. Sound Vib.*, **332**(19), pp. 4656–4667.
- [80] Abdelkefi, A., Hajj, M. R., and Nayfeh, A. H., 2013, “Piezoelectric Energy Harvesting from Transverse Galloping of Bluff Bodies,” *Smart Mater. Struct.*, **22**(1).
- [81] Sun, W., Tan, T., Yan, Z., Zhao, D., Luo, X., and Huang, W., 2018, “Energy Harvesting from Water Flow in Open Channel with Macro Fiber Composite,” *AIP Adv.*, **8**(9).
- [82] Dellinger, N., François, P., Lefebure, D., Mose, R., and Garambois, P. A., 2018, “An Experiment of a Hydropower Conversion System Based on Vortex-Induced Vibrations in a Confined Channel,” *Renew. Energy*, **115**, pp. 54–63.
- [83] Neo, R. G., and Khoo, B. C., 2021, “A Study on the Design Parameters for Water–Solid Triboelectric Energy Harvesting with a Channel Device,” *Sustain. Energy Technol. Assessments*, **47**(June).
- [84] Goushcha, O., Akaydin, H. D., Elvin, N., and Andreopoulos, Y., 2015, “Energy Harvesting Prospects in Turbulent Boundary Layers by Using Piezoelectric Transduction,” *J. Fluids Struct.*, **54**, pp. 823–847.
- [85] Sun, W., Liu, C., Hu, S., Liu, Y., and Zhao, D., 2023, “Enhancing/Diminishing Piezoelectric Energy Harvesting by Adjusting the Attachment Height,” *Ocean Eng.*, **269**(January), p. 113700.
- [86] Zheng, X., He, L., Wang, S., Liu, X., Liu, R., and Cheng, G., 2023, “A Review of Piezoelectric Energy Harvesters for Harvesting Wind Energy,” *Sensors Actuators A Phys.*, **352**(October 2022), p. 114190.
- [87] Wu, N., Bao, B., and Wang, Q., 2021, “Review on Engineering Structural Designs for Efficient Piezoelectric Energy Harvesting to Obtain High Power Output,” *Eng. Struct.*, **235**(February), p. 112068.
- [88] Hamlehdar, M., Kasaeian, A., and Safaei, M. R., 2019, “Energy Harvesting from Fluid Flow Using Piezoelectrics: A Critical Review,” *Renew. Energy*, **143**, pp. 1826–1838.
- [89] Saeed, M., Uddin, E., Mubashar, A., Zahir, S. U., and Zaidi, A. A., 2018, “Design and Development of Low-Speed Water Tunnel,” *Proc. 2018 15th Int. Bhurban Conf. Appl. Sci. Technol. IBCAST 2018*, **2018-Janua**(January), pp. 614–619.
- [90] Choi, C. K., and Kwon, D. K., 1998, “Wind Tunnel Blockage Effects on Aerodynamic Behavior of Bluff Body,” *Wind Struct. An Int. J.*, **1**(4), pp. 351–364.
- [91] Michelin, S., and Doaré, D., 2013, “Energy Harvesting Efficiency of Piezoelectric Flags in Axial Flows,” *J. Fluid Mech.*, **714**, pp. 489–504.
- [92] Orrego, S., Shoele, K., Ruas, A., Doran, K., Caggiano, B., Mittal, R., and Kang, S. H., 2017, “Harvesting Ambient Wind Energy with an Inverted Piezoelectric Flag,” *Appl. Energy*, **194**, pp. 212–222.
- [93] Li, Z., Yao, W., Yang, K., Jaiman, R. K., and Khoo, B. C., 2016, “On the Vortex-Induced Oscillations of a Freely Vibrating Cylinder in the Vicinity of a Stationary Plane Wall,” *J. Fluids Struct.*, **65**, pp. 495–526.
- [94] Ryu, J., Park, S. G., Kim, B., and Sung, H. J., 2015, “Flapping Dynamics of an Inverted Flag in a Uniform Flow,” *J. Fluids Struct.*, **57**, pp. 159–169.

- [95] Sciences, P., 1964, "The Lift and Drag Forces on a Circular Cylinder in a Flowing Fluid
Author (s): R . E . D . Bishop and A . Y . Hassan Source : Proceedings of the Royal
Society of London . Series A , Mathematical and Published by : Royal Society Stable
URL : <https://www.royalsocietypublishing.org/journal/rsos>," **277**(1368), pp. 32–50.